Drug Design, Development and Therapy

Dovepress
Taylor & Francis Group

Open Access Full Text Article

ORIGINAL RESEARCH

Cornus officinalis Protects Against Steroid-Induced Osteonecrosis of the Femoral Head Through Inhibiting Inflammatory Responses and Apoptosis via Network Pharmacology and Experimental Validation

Ying Wang[1], Yuhang Fan[2], Mengjiao Li[2], Zheming Song[2], Pengcheng Wang[3], Fei Xie[4], Yuqi Miao[2], Yifan Wang[5], Peng Zhang[5,*], Qiang Zhan[6,*]

[1]Department of Pharmacy, Hangzhou Red Cross Hospital, Hangzhou, Zhejiang, People's Republic of China; [2]The Second School of Clinical Medicine, Zhejiang Chinese Medical University, Hangzhou, Zhejiang, People's Republic of China; [3]Department of Tuberculosis, Hangzhou Red Cross Hospital, Hangzhou, Zhejiang, People's Republic of China; [4]Department of Otolaryngology, Hangzhou Red Cross Hospital, Hangzhou, Zhejiang, People's Republic of China; [5]Department of Orthopedic, Hangzhou Red Cross Hospital, Hangzhou, Zhejiang, People's Republic of China; [6]Department of Massage, Hangzhou Red Cross Hospital, Hangzhou, Zhejiang, People's Republic of China

*These authors contributed equally to this work

Correspondence: Qiang Zhan, Department of Massage, Hangzhou Red Cross Hospital, Hangzhou, Zhejiang, People's Republic of China, Email zqtow@163.com; Peng Zhang, Department of Orthopedic, Hangzhou Red Cross Hospital, Hangzhou, Zhejiang, People's Republic of China, Email zhangpbs2017@163.com

Background: Steroid-related osteonecrosis of the femoral head (SONFH) is bone death resulting from the use of chronic glucocorticoids. Due to its high incidence and lack of effective treatment, which is still a challenging problem in orthopedic surgery. Cornus officinalis (SZY) is usually used as a traditional use for the treatment of SONFH and plays a major role in traditional prescriptions, however, the specific pharmacological mechanisms of action remain unclear. This study is to investigate the mechanisms of SZY against SONFH via network pharmacology and experimental validation analysis.

Methods: The active components and related targets of SZY and related-SONFH targets were collected from public databases. The protein–protein interaction (PPI) network, Gene Ontology (GO) and Kyoto Encyclopedia of Genes and Genomes (KEGG) functional enrichment analyses were performed to predict the core targets and pathways of SZY in the treatment of SONFH. Then, AutoDock Vina was used for molecular docking verification. Finally, the reliability of the network pharmacology prediction results was verified through a mice SONFH model in vivo experiment.

Results: Through the identification of common targets between the active components of SZY and targets related to SONFH, a total of 66 shared targets were identified. The topological analysis of the PPI network identified nine key targets. GO and KEGG enrichment analyses showed that SZY treatment for SONFH mainly include apoptosis and IL-17 signaling pathways. Molecular docking and molecular dynamics simulations results indicated that the active components in SZY exhibited high affinity for these targets. Animal experiments demonstrated that SZY reduced femoral head damage in SONFH mice, significantly downregulating TNF ($p<0.01$) and IL-6 ($p<0.05$) and modulating Bcl-2/Caspase-3 expression.

Conclusion: Our study provides preclinical evidence that SZY alleviates SONFH by suppressing inflammation and apoptosis, supporting its traditional use and informing further translational research.

Keywords: steroid-related osteonecrosis of the femoral head, cornus officinalis, network pharmacology, molecular mechanisms, apoptosis, inflammation

Introduction

Steroid-induced necrosis of the femoral head (SONFH) is a recalcitrant orthopedic condition triggered by inappropriate administration of glucocorticoids in clinical practice, culminating in the gradual demise of osseous cells and bone

Received: 3 February 2025
Accepted: 19 June 2025
Published: 9 July 2025

marrow, ultimately culminating in localized ischemic necrosis and subsequent joint surface collapse.[1–3] SONFH has a high disability rate and significantly impacts the quality of life of individuals. It not only leads to health losses for patients, but also causes social burden and economic losses.[4,5] Current therapeutic approaches for SONFH including corticosteroids, core decompression (CD) and vascularized bone grafting (VBG), demonstrate clinical potential but are constrained by significant limitations. Meanwhile, emerging interventions such as stem cell therapy and vascular transplantation have garnered increasing attention due to their therapeutic promise.[6,7] However, the widespread clinical implementation of these advanced treatments faces substantial challenges, including prohibitive costs, technical complexities, and inconsistent patient responses. Clinical data shows that without effective intervention, 90% of patients with femoral head necrosis will experience femoral head collapse within five years, typically requiring total hip arthroplasty (THA).[8,9] Nevertheless, due to the limited lifespan of prostheses and the high risk of complications from multiple revision surgeries, THA is not ideal for young patients. Thus, it is crucial to discover potential drugs with significant efficacy and efficient treatment for SONFH. Nevertheless, the contemporary understanding of the pathophysiology of SONFH has not been fully explored, which seriously affects the research of disease diagnosis and treatment.[10,11] Recent investigations have revealed that the pathogenesis of SONFH is multifactorial, lipid metabolism disorders and osteoblast death believed to play a crucial role in the development and progression of SONFH.[12,13]

The fruit of cornus officinalis (SZY) is a food with both medicinal and edible properties, as well as a traditional Chinese medicinal herb. In the context of TCM, it is believed that SZY has effects of nourishing the liver and kidney, which may correlate with SZY's modulation of inflammatory pathways and bone remodeling processes.[14] This is the theoretical basis for SZY delaying the progression of SONFH. Traditional Chinese medicine (TCM) has a longstanding history of treating SONFH. In recent years, numerous scholars have conducted extensive research on the effectiveness of TCM in the treatment of SONFH, employing a molecular biology approach.[15] Their research results have proven that TCM exhibits favorable therapeutic effect on treating SONFH with fewer side effects.[16,17] Recent pharmacological research has shown that SZY primarily improves bone microstructure, stimulates osteogenesis, and enhances blood perfusion in the bone marrow.[18] The active constituents of SZY demonstrate significant promise for the advancement of innovative pharmaceuticals for the treatment of SONFH.[19] According to previous experimental studies, SZY can effectively suppresses osteoclast differentiation induced by RANKL through the inhibition of NF-KB activity.[20] Oral administration of SZY and achyranthes japonica mixture can also significantly prevent the loss of bone mineral density and maintain trabecular bone structures.[21] Moreover, unlike long-term glucocorticoids, SZY has fewer adverse reactions. Although SZY has demonstrated potential therapeutic effects in the treatment of SONFH, existing researches have only focused on the mechanism of a single target, lacking a comprehensive and systematic overall study. Therefore, the exact mechanism of SZY in the treatment of SONFH is still unclear, which hinders its wider clinical application. Consequently, it is imperative to further study the molecular mechanism of SZY.

Network pharmacology is a systematic research methodology that employs a variety of techniques, including database screening, computer simulation, and information mining, to effectively identify therapeutic targets, forecast signaling pathways and mechanisms of action, and clarify the biological foundations of diseases.[22,23] By constructing the network relationship between the active ingredients of TCM and its target proteins, network pharmacology can clarify the inherent multi-target mechanism of TCM. Its holistic nature aligns well with approach of TCM.[23,24] Therefore, network pharmacology is particularly suitable for exploring the pharmacological basis and holistic therapeutic mechanisms of SZY in treating SONFH.[25] Molecular docking is a computational technology, which makes the rational design of therapeutic drugs possible by verifying predicted ligand-receptor interactions from network analysis. It is of great significance to develop novel drugs with enhanced efficacy and reduced side effects for the treatment of various diseases.[25]

This research utilized a network pharmacology methodology in combination with in vivo experimental verification to investigate the potential targets, signaling pathways, and molecular mechanisms of SZY in the management of SONFH. We hypothesize that SZY mitigates SONFH by synergistically targeting inflammatory and apoptotic pathways. The findings of this study could offer a novel strategy for advancement of pharmaceuticals and biological agents for the prevention and treatment of SONFH. It also may inform the development of SZY-based therapeutics for clinical SONFH management. Figure 1 illustrated the methodology of this study.

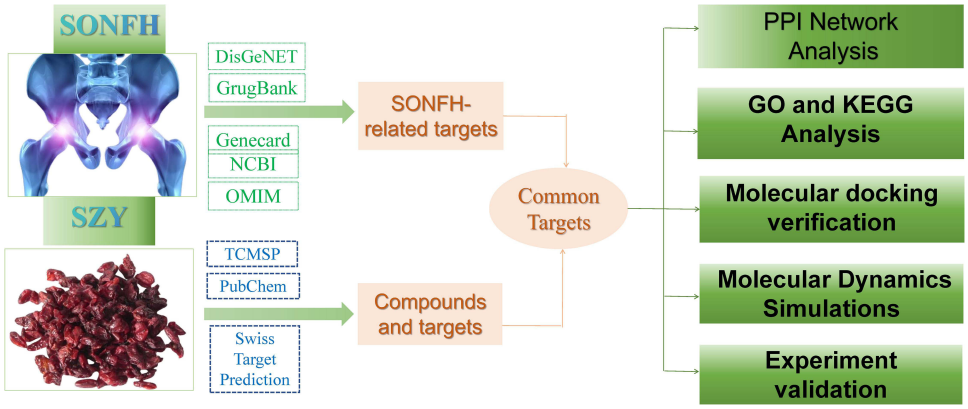

Figure 1 Workflow of the network pharmacological investigation strategy of SZY in the treatment of SONFH.

Materials and Methods

Materials and Reagents

Cornus officinalis (SZY) were purchased from Hangzhou Red Cross Hospital and identified as authentic by Prof. Wang Yan and conformed to the specifications of the 2020 edition of the Pharmacopoeia of the People's Republic of China (The specimen of *Cornus officinalis* can refer to the website: https://www.cvh.ac.cn/spms/detail.php?id=b65b100b). Primary antibodies against Bcl-2 (ab194583), IL-6 (ab290735), and TNF-α (ab307164) were procured from Abcam Company Ltd. (Cambridge, MA, USA), while the primary antibody against Caspase-3 (ER30804) was obtained from Hua'an Biological Co. (Hangzhou, China). The goat anti-rabbit Alexa Fluor 488 secondary antibody (#4412) was sourced from Cell Signaling Technology (Beverly, MA, USA). TUNEL Bright Green Apoptosis Detection Kit (4812–30-K) was supplied by R&D (R&D Systems, MN, United States).

UPLC-Q-TOF-MS of SZY

The analysis was conducted using a Waters UPLC system (Waters Corp., Milford, MA, USA) in conjunction with an AB Triple TOF 6600plus system (AB SCIEX, Framingham, USA). The chromatographic conditions included a mobile phase consisting of 0.1% formic acid-water for mobile phase A and 0.1% formic acid-acetonitrile for mobile phase B. The separation was achieved using an ACQUITY UPLC T3 column (1.8μm, 2.1×150 mm; Waters Corp.) with a gradient elution profile of 0–22 min at 5–35% B and 22–37 min at 35–95% B. The column oven temperature was maintained at 50°C, with a flow rate of 0.3 mL•min^{-1} and a sample injection volume of 3μL.

Network Pharmacology

The identification and selection of the components and therapeutic targets of SZY.

The active components of SZY were obtained from the Traditional Chinese Medicine Systems Pharmacology (TCMSP) database.[26] Selection criteria for potential active components included meeting the ADME pharmacokinetic properties outlined in the TCMSP database, specifically oral bioavailability (OB) ≥30% and drug-likeness property (DL) ≥0.18.[27] The TCMSP was utilized to predict the potential targets of these bioactive components. Subsequently, the obtained potential targets were mapped to gene symbols using the UniProtKB database.[28] The PubChem and the Swiss Target Prediction Tools were also utilized to collect potential targets of the bioactive components in SZY.[29]

Disease Target Screening

Disease targets associated with SONFH were explored from 5 databases, including GeneCards,[30] the OMIM database,[31] the DisGeNET database,[32] the GrugBank database[33] and the NCBI database.[34] These databases contain data pertaining to human genes and genetic disorders and potential therapeutic targets for various diseases. This research is conducted using legally available public data, which meets the requirements of Article 32, item 1 of the Measures for Ethical Review of

Life Science and Medical Research Involving Human Subjects dated February 18, 2023, China, and could be exempted from ethical approval. Through searching the key word "osteonecrosis of the femoral head", specific disease targets associated with SONFH were discerned following the elimination of duplicate targets. The overlap between SZY targets and SONFH-related disease targets is considered to be the potential targets for SZY to treat SONFH.

Establishment of PPI Network

The overlap targets were submitted to the STRING database to generate a PPI network.[35] The analysis was limited to the biological species "*Homo sapiens*" with a confidence score of at least 0.4. Cytoscape version 3.7.2 was used to visualize the PPI network.[36] The MCODE plugin was utilized to analyze the correlation among network clusters and identify hub genes with high connectivity.[37] A topological examination of the PPI network was conducted, adjusting the size and color of nodes based on their degree. Filter parameters were set to values exceeding the average degree and twice the median value. Additionally, the Cytohubba plugin employing the Maximum Clique Centrality (MCC) algorithm was used to further refine the PPI network.[38] The intersection targets of three screening methods are considered key targets.

GO and KEGG Enrichment Analyses

The DAVID database was employed to the outcomes of the GO and KEGG pathway enrichment analyses were refined using a significance threshold of $P < 0.05$ and FDR <0.05. The GO function analysis encompassed three distinct categories of GO terms: biological process (BP), cellular component (CC), and molecular function (MF).[39] Visual representations of the top 10 Gene Ontology terms and top 20 KEGG pathway results with the highest statistical significance were generated using the R platform. Furthermore, a network consisting of herb-component-target-pathway was created using Cytoscape 3.7.2 to reveal the complex relationships among the top 20 KEGG pathways, their corresponding targets, and component.

Molecular Docking Verification

Molecular docking technology was employed for the examination of component-target interactions, as well as the prediction of their affinity and binding configurations. We selected the 8 key targets derived from PPI network analysis and the top 10 components with the highest degree of herb-component-target-pathway network for molecular docking validation. Initially, the conformational information and 3D structural format files of the components were retrieved and downloaded from the PubChem database.[40] Then retrieve the crystal structure of the protein target from the RSCB PDB database and download the PDB format file.[41] Subsequently, AutoDockTools was used to preprocess the crystal structure of the target protein, including removing excess protein chains, dehydration, hydrogenation.[42] The docking grid box was subsequently constructed in AutoDockTools to obtain the position and size of the active pocket where the original co crystalline ligands were located in the protein structure.[43] The ligand structure is optimized to achieve a low-energy conformation, and the ligand and receptor are processed into PDBQT format. In addition, we used AutoDock Vina 4.2 to simulate the docking interaction between ligands and proteins, setting the exhaustion settings to.[44,45] After the docking is completed, we will re dock the extracted co crystalline ligand with the protein at the original pocket position to verify the reliability of the docking results. Finally, the molecular docking analysis results were visualized using Discovery Studio 2020 and PyMOL software.

Molecular Dynamics Simulations

Molecular dynamics (MD) simulations of the complexes were conducted utilizing the Gromacs 2022 software suite.[46] The CHARMM36 force field was applied to model the proteins, while the GAFF2 force field was employed for the ligands.[47] The system was solvated using the TIP3P water model within a periodic boundary box, extending 1.2 nm from the protein-ligand complex. For the treatment of electrostatic interactions, the Particle Mesh Ewald (PME) method was implemented in conjunction with the Verlet cutoff scheme.[48] The system underwent energy minimization, followed by two equilibration phases: 100 ps of NVT (canonical ensemble) equilibration and 100 ps of NPT (isothermal-isobaric ensemble) equilibration, both utilizing a coupling constant of 0.1 ps. Van der Waals and Coulomb interactions were computed with a cutoff distance of 1.0 nm. Subsequently, the system was simulated using Gromacs 2022 under conditions of constant temperature (310 K) and constant pressure (1 bar) for a duration of 100 ns.[49]

Experimental Validation

Experimental Animal and Groups

Forty healthy female C57/BL6 mice, aged 10 weeks and weighing 20 to 22 grams, were obtained from the animal center of Zhejiang Chinese Medical University. The mice underwent a 7-day acclimation period in a controlled environment with appropriate light intensity and humidity, and were given unrestricted access to food and water before the commencement of treatment. All research and procedures for animal experiments were performed in accordance with the International Guide for the Care and Use of the Laboratory Animals and approved by the Animal Experimental Ethics Committee of Zhejiang Chinese Medicine University (IACUC-20230731-01). All mice were randomly allocated to one of four groups: the control group, the SONFH-model group, the SZY-low group and the SZY-high group (N=10 per group). The SONFH model was developed based on prior research.[50] In brief, mice in the SONFH and SZY groups received two intravenous injections of lipopolysaccharide (LPS; 20 μg/kg, Sigma, USA) on day 0. Subsequently, three intramuscular injections of 40 mg/kg body weight of methylprednisolone (MPS; Pfizer, USA) were administered at 24-hour intervals after 24 hours (Figure 2A). The mice in the SZY group were administered SZY at doses of 7.5 g/kg/d and 15 g/kg/d for a duration of 6 weeks. The specific

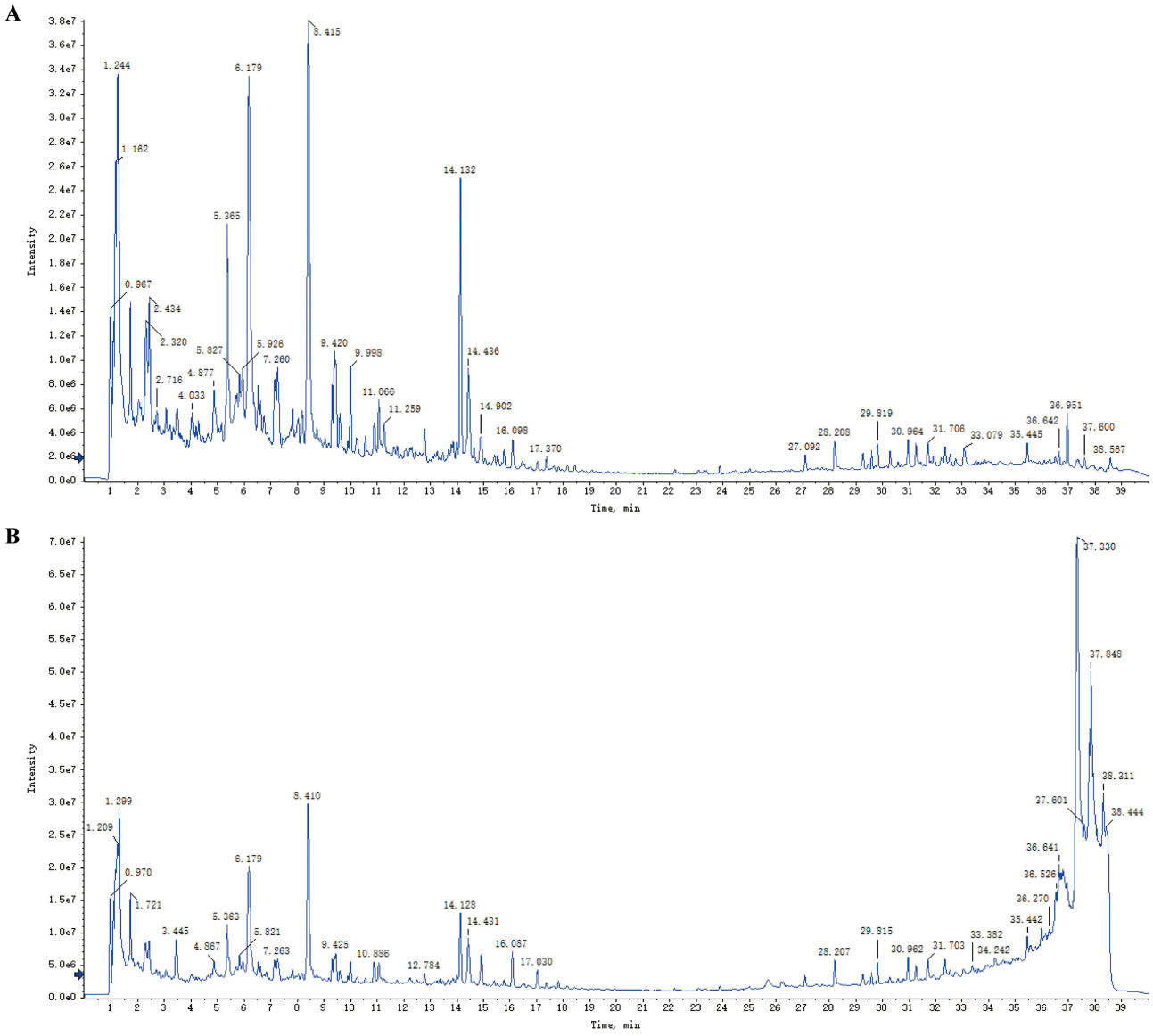

Figure 2 LC-Q-TOF/MS analysis of SZY. (**A**) Total ion chromatogram of SZY in negative ion mode; (**B**) Total ion chromatogram of SZY in positive ion mode.

https://doi.org/10.2147/DDDT.S518115

oral dosage was determined using a conversion formula. The mice in the SONFH group received an equivalent dose of 0.9% normal saline.

Histopathological Analysis

After 6 weeks from the last injection of MPS, mice were humanely euthanized using an overdose of pentobarbital sodium, and bilateral femurs were harvested post-mortem. Subsequently, the right femur was immersed in a 4% paraformaldehyde solution (pH 7.4) for a duration of 3 days in preparation for micro-computed tomography (micro-CT) analysis. Following micro-CT scanning, the bone specimens underwent decalcification in a 10% ethylenediaminetetraacetic acid (EDTA, pH 7.4) solution for approximately 30 days. Following embedding in paraffin, the sample was cut along the coronal plane into 4μm-thick sections, which were subsequently stained with Alcian Blue/Hematoxylin (ABH) and counterstained with Eosin/Orange G. Subsequently, the sample was digitally scanned utilizing the Olympus VS-120 whole slide imaging system.[51] Histopathological analysis was conducted to investigate osteonecrosis lesions in mice treated with steroids. The assessment of osteonecrosis followed the criteria established in the study by Yamamoto et al.[52] Osteonecrosis was identified through the assessment of necrosis in medullary hematopoietic cells or adipocytes, reduced bony trabeculae, empty lacunae, or pyknotic nuclei in osteocytes. Additionally, the quantification of vacant lacunae and pyknotic nuclei was conducted for each femoral head.

Micro-CT Analysis and Mechanical Test

Prior to histological processing, the vertebrae that had been preserved with paraformaldehyde were analyzed using micro-CT technology.[53] The Skyscan 1176 micro-CT instrument (Bruker, Kontich, Belgium) was used to scan the separated femurs of each group with a resolution of 4000×2672 pixels and an isotropic voxel size of 10 mm. NRecon and CTAn software were utilized for image reconstruction and analysis, respectively. Additionally, CTVol, a software for visualizing three-dimensional models, was employed for structural image assessment and analysis of femoral head parameters. A 3D reconstruction and analysis were conducted on 10 consecutive images of the femoral head to assess the parameters of bone trabecular volume per total tissue volume (BV/TV), trabecular thickness (Tb.Th), and trabecular separation (Tb.Sp).

Immunohistochemistry (IHC) Analyses and Immunofluorescence (IF) Analyses

In the context of the IF assay, tissue sections were exposed to primary antibodies targeting Bcl-2 (at a dilution of 1:300), Caspase-3 (at a dilution of 1:300), IL-6 (at a dilution of 1:500), and TNF-α (at a dilution of 1:500) at a temperature of 4° C for an overnight incubation period. Following the initial procedures, immunohistochemistry (IHC) analysis was conducted using a secondary biotinylated goat anti-rabbit antibody (diluted at 1:1000) sourced from Invitrogen, applied for a duration of 30 minutes on the subsequent day. The detection of immunohistochemically staining was achieved using a diaminobenzidine solution (Invitrogen), followed by counterstaining with hematoxylin. In the immunofluorescence analysis, a secondary goat anti-rabbit antibody conjugated with a fluorophore (diluted at 1:1000) was administered for 30 minutes on the second day. The quantification of positive cells was conducted using Image Pro Plus 6.0 in a double-blind fashion, as detailed in our previous work.[54,55]

TUNEL Staining

TUNEL staining was conducted on paraffin-embedded sections utilizing an in situ cell death detection kit, followed by counterstaining with hematoxylin. Quantification entailed the enumeration of TUNEL-positive cells in five randomly chosen fields per slide at a 200x magnification, with subsequent calculation of the average values. Apoptosis was evaluated by determining the ratio of TUNEL-positive cells to the total cell count.

Statistical Analysis

Statistical analysis was performed utilizing SPSS software (version 25.0, Chicago, Illinois, USA), with data reported as mean±standard deviation. The analysis encompassed a one-way ANOVA test and independent sample *t*-test. Tukey multiple analysis was performed using Graph pad Prism 7. The value of $P<0.05$ was regarded as a statistically significant difference.

Results

Component Analysis of SZY

The representative total ion chromatograms (TICs) of SZY obtained using LC-Q-TOF/MS in positive and negative ion modes are presented in Figure 2. The raw TIC data was processed using PeakView 2.2 software, resulting in the identification of 108 chemical components in SZY. The mass spectrometry data was analyzed by comparing it to the 1.0 database of Natural Products HR-MS/MS Spectral Library in order to identify compounds. Components were first screened based on chromatographic peak scores and subsequently verified using primary and secondary information for each component. In total, 26 components were identified from SZY. Detailed information on each component, including measured mass, calculated mass, substance type, and structure, is presented in Table 1.

Screening the Components and Therapeutic Targets of SZY

Totally, 20 chemical components of SZY were obtained from TCMSP databases (Supplementary Table 1). A total of 600 targets associated with 20 active components of SZY were identified through a search in the TCMSP database target module and the Swiss Target Prediction Tools, with redundant targets removed (Supplementary Table 2). Integration of SONFH-related targets from various databases yielded a total of 589 targets after eliminating duplicates (Figure 3A). By comparing the SZY components targets and SONFH-related targets, 66 intersection targets were identified (Figure 3B and Supplementary Table 3).

PPI Network of Common Targets

To investigate the underlying mechanism of SZY's therapeutic effectiveness in the treatment of SONFH, we utilized the STRING database and Cytoscape 3.7.2 software to create a PPI network comprising 66 common targets. The PPI network revealed the interplay among putative therapeutic targets, featuring 66 nodes and 600 edges (Figure 4A). The nodes within the graph exhibit a progression in both color and size, shifting from lighter and smaller nodes to larger and darker nodes, signifying a rise in the degree value of the nodes from lower to higher values. A cluster analysis was conducted using MCODE and the 66 targets were divided into 3 groups. Module 1 has 25 nodes, 242 edges and a score of 20. 167. Additionally, a more in-depth topology analysis of the protein-protein interaction network identified 10 core targets based on a degree centrality greater than twice the median degree centrality (Figure 4B). In addition, the top 10 genes were identified utilizing the MCC method within the CytoHubba plug-in, as illustrated in Figure 4C. The intersection targets of MCODE, topology analysis and MCC methods were considered key targets of the PPI network (Figure 4D). Ultimately, a total of 9 key targets (including TNF, TP53, EGFR, CASP3, HIF1A, PPARG, ESR1, SRC, TGFβ1) were identified, suggesting their potential importance in the treatment of SONFH.

GO and KEGG Enrichment Analysis

In order to elucidate the biological mechanisms of SZY in relation to SONFH, GO and KEGG pathway enrichment analysis was performed. A total of 413 GO terms that were enriched, with 288 terms associated with BP, 50 terms related to CC, and 75 terms related to MF. These results are shown in Supplementary Table 4–6. The top 3 GO-BP terms were negative regulation of apoptotic process, positive regulation of pri-miRNA transcription from RNA polymerase II promoter and positive regulation of apoptotic process. The three most enriched GO-CC terms were mainly enriched in membrane raft, membrane raft receptor complex, extracellular space. Additionally, the analysis indicated that the top three GO-MF terms primarily pertained to enzyme binding, steroid binding, p53 binding. The top ten enriched BP, MF, and CC terms were identified and presented visually through a bubble chart and bar diagram, as depicted in Figure 5A and B. According to the results of the GO-BP terms, it is suggested that the apoptotic process may have a substantial impact on the mechanism of SZY in the treatment of SONFH.

Additionally, a KEGG pathways enrichment analysis was conducted to investigate the potential functions of the targets ($P < 0.05$ and FDR < 0.05), resulting in a total of 88 KEGG enrichment entries (Supplementary Table 7). The top 20 significantly enriched pathways were identified based on their P-values and presented in Table 2, Figure 6A and B. A Sankey diagram was generated to visually represent the connections among the enriched pathways (Figure 6C). The

Table 1 Results of the Identification of the Main Components of SZY

NO.	RT (min)	Name	Formula	Expected m/z	Found at m/z	Error (ppm)	Type of Substance	CAS NO.	Structure
1	1.2	Tartaric acid	C4H6O6	149.0092	149.01	5.4	Acyclic	87–69-4	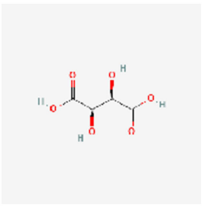
2	1.23	4-methyl-5,6-dihydro-2H-pyran-2-one	C6H8O2	111.0452	111.0453	0.9	Heterocyclic	2381–87-5	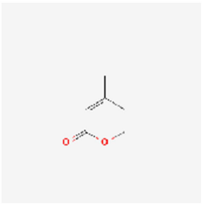
3	2.44	Gallic acid	C7H6O5	169.0142	169.0154	6.9	Isocyclic	149–91-7	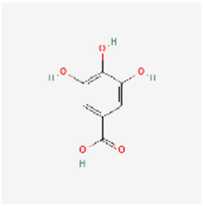
4	2.44	5-hydroxymethylfurfural	C6H6O3	125.0244	125.0254	7.8	Heterocyclic	77–52-1	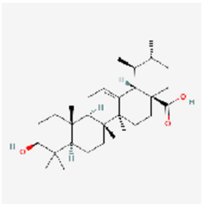
5	2.94	Gemin D	C27H22O18	633.0733	633.0745	1.8	Heterocyclic		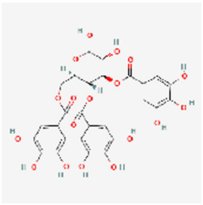

(*Continued*)

Table 1 (Continued).

NO.	RT (min)	Name	Formula	Expected m/z	Found at m/z	Error (ppm)	Type of Substance	CAS NO.	Structure
6	5.11	Salidroside	C14H20O7	299.1136	299.1133	−0.9	Heterocyclic	10338–51-9	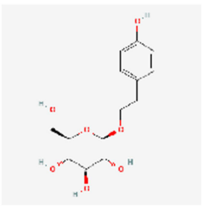
7	6	(4R)-4-methyltetrahydro-2H-pyran-2-one	C6H10O2	113.0608	113.0609	0.8	Heterocyclic	61898–55-3	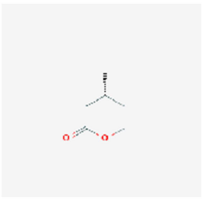
8	6.13	Loganin	C17H26O10	389.1453	389.1452	−0.2	Heterocyclic	18524–94-2	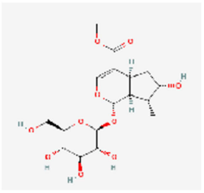
9	6.18	Myo-inositol	C6H12O6	179.0561	179.0563	0.9	Isocyclic	488–59-5	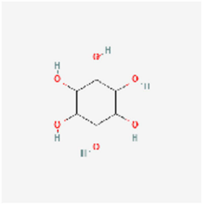
10	7.34	β-(3,4-dihydroxyphenyl)-ethyl-O-β-D-glucopyranoside	C14H20O8	315.1085	315.1087	0.6	Heterocyclic	76873–99-9	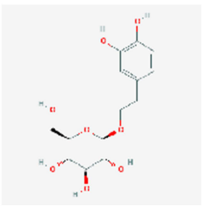

(*Continued*)

https://doi.org/10.2147/DDDT.S518115

Table 1 (Continued).

NO.	RT (min)	Name	Formula	Expected m/z	Found at m/z	Error (ppm)	Type of Substance	CAS NO.	Structure
11	7.65	Tellimagrandin II	C41H30O26	937.0953	937.0901	−5.4	Heterocyclic	1268481–34-0	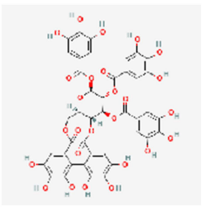
12	8.19	1,2,3-tri-O-galloyl-β-D-glucopyranose	C27H24O18	635.089	635.0901	1.7	heterocyclic		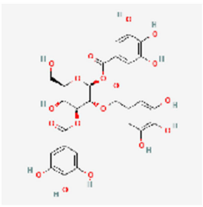
13	8.39	Secoxyloganin	C17H24O11	403.1246	403.1251	1.3	Heterocyclic	58822–47-2	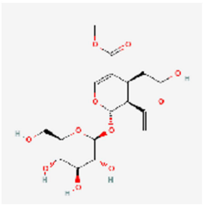
14	8.39	Sweroside	C16H22O9	357.1191	357.1189	−0.6	Heterocyclic	14215–86-2	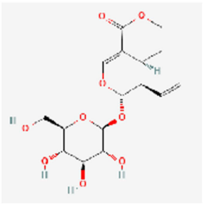
15	9	Hydroxytyrosol	C8H10O3	153.0557	153.0557	0.1	Isocyclic	10597–60-1	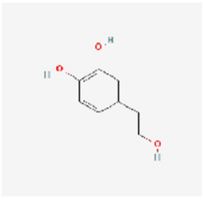

(*Continued*)

Table 1 (Continued).

NO.	RT (min)	Name	Formula	Expected m/z	Found at m/z	Error (ppm)	Type of Substance	CAS NO.	Structure
16	10.31	1,2,3,6-tetra-O-galloyl-β-D-glucose	C34H28O22	787.0999	787.1013	1.7	Heterocyclic		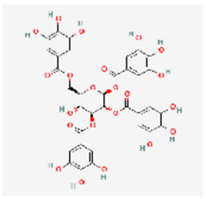
17	10.41	Catechin	C15H14O6	289.0718	289.0719	0.4	Heterocyclic	154–23-4	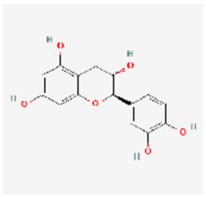
18	11.18	Quercetin 3-O-β-D-glucuronopyranoside	C21H18O13	477.0675	477.0678	0.7	Heterocyclic		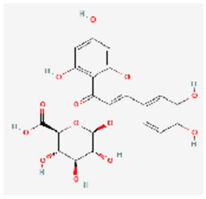
19	11.62	Isoquercetin	C21H20O12	463.0882	463.0884	0.5	Heterocyclic	482–35-9	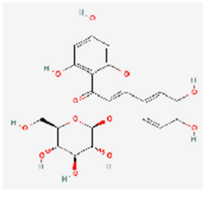
20	13.04	Avicularin	C20H18O11	433.0776	433.0775	−0.2	Heterocyclic	549–32-6	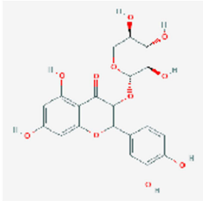

(*Continued*)

https://doi.org/10.2147/DDDT.S518115

Table 1 (Continued).

NO.	RT (min)	Name	Formula	Expected m/z	Found at m/z	Error (ppm)	Type of Substance	CAS NO.	Structure
21	13.8	Quercitrin	C21H20O11	447.0933	447.0929	−0.8	Heterocyclic	522–12-3	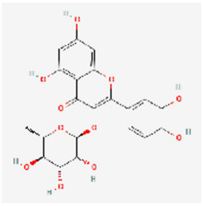
22	17.96	quercetol	C15H10O7	301.0354	301.0356	0.8	heterocyclic	117–39-5	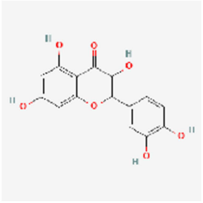
23	25.8	23-hydroxytormentic acid	C30H48O6	503.3378	503.3378	0	Isocyclic		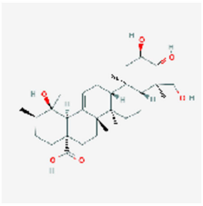
24	28.21	Arjunolic acid	C30H48O5	487.3429	487.3434	1	Isocyclic		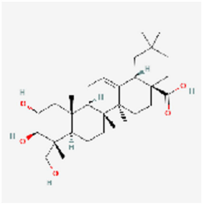
25	32.55	Alphitolic acid	C30H48O4	471.348	471.3484	0.8	Isocyclic		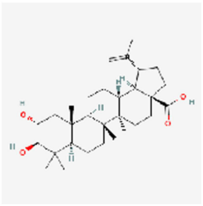

(*Continued*)

Table 1 (Continued).

NO.	RT (min)	Name	Formula	Expected m/z	Found at m/z	Error (ppm)	Type of Substance	CAS NO.	Structure
26	36.22	Ursolic acid	C30H48O3	455.3531	455.3535	0.9	Isocyclic	77–52-1	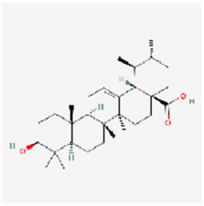

selection of the top 20 pathways was made in order to construct a component-target-pathway network comprising 105 nodes and 500 edges using Cytoscape 3.7.2 (Figure 6D). Examination of KEGG enrichment revealed that pathways related to apoptosis, IL-17 signaling, estrogen signaling, and thyroid hormone signaling were deemed statistically significant. Notably, the apoptosis pathway emerged as pivotal in the context of SONFH (Figure 6E).

Molecular Docking Verification

In the herb-component-target-pathway network, a selection was made of the top ten components and eight key targets for molecular docking verification. The details pertaining to the targets and components, as well as the spatial coordinates of docking, are provided in Supplementary Table 8. Figure 7 illustrates the binding energies of the principal targets and active components, as well as the results of redocking. The outcomes of the docking procedure indicate that the principal targets typically exhibited favorable docking interactions with the active components. It is commonly accepted that a lower docking binding energy corresponds to a more stable conformation. Therefore, molecular docking complexes were selected based on a binding energy below −9 kcal/mol to elucidate their docking modes (Figure 8). Notably, among these complexes, PPARG-stigmasterol displayed the most favorable binding energy of −10.1 kcal/mol. The binding mode of PPARG-stigmasterol revealed the formation of a hydrogen bond with the amino acid residue Glu-272. TNF-stigmasterol form a hydrogen bond with Glu-116 residue and exhibit −9.8 kcal/mol binding affinity. CASP3-beta-sitosterol form a hydrogen bond with Thr-140 residue and exhibit −9.7 kcal/mol binding affinity. The TNF and CASP3 proteins, along with their respective active compounds, form stable complexes with high docking performance. Examples of these stable complexes include CASP3-poriferast-5-en-3beta-ol (−9.7kcal/mol), CASP3-stigmasterol (−9.5kcal/mol), CASP3-sitosterol (−9.5kcal/mol), TNF-sitosterol (−9.5 kcal/mol), TNF-beta-sitosterol (−9.1 kcal/mol). These interactions are facilitated by strong hydrogen bonding, Pi-sigma interactions, and/or Pi-Alkyl stacking.

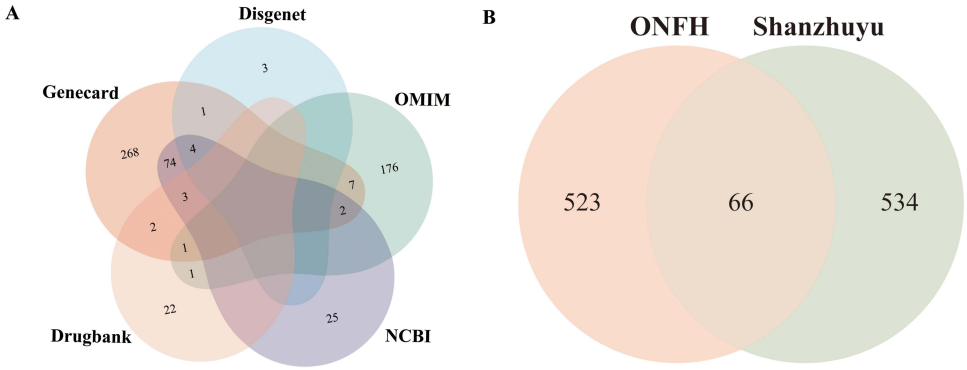

Figure 3 Screening of SZY-SONFH common targets. (**A**) The intersection of disease targets in various databases. (**B**) Venn diagram of the 66 common targets between the active compounds targets of SZY and the disease targets of SONFH.

https://doi.org/10.2147/DDDT.S518115

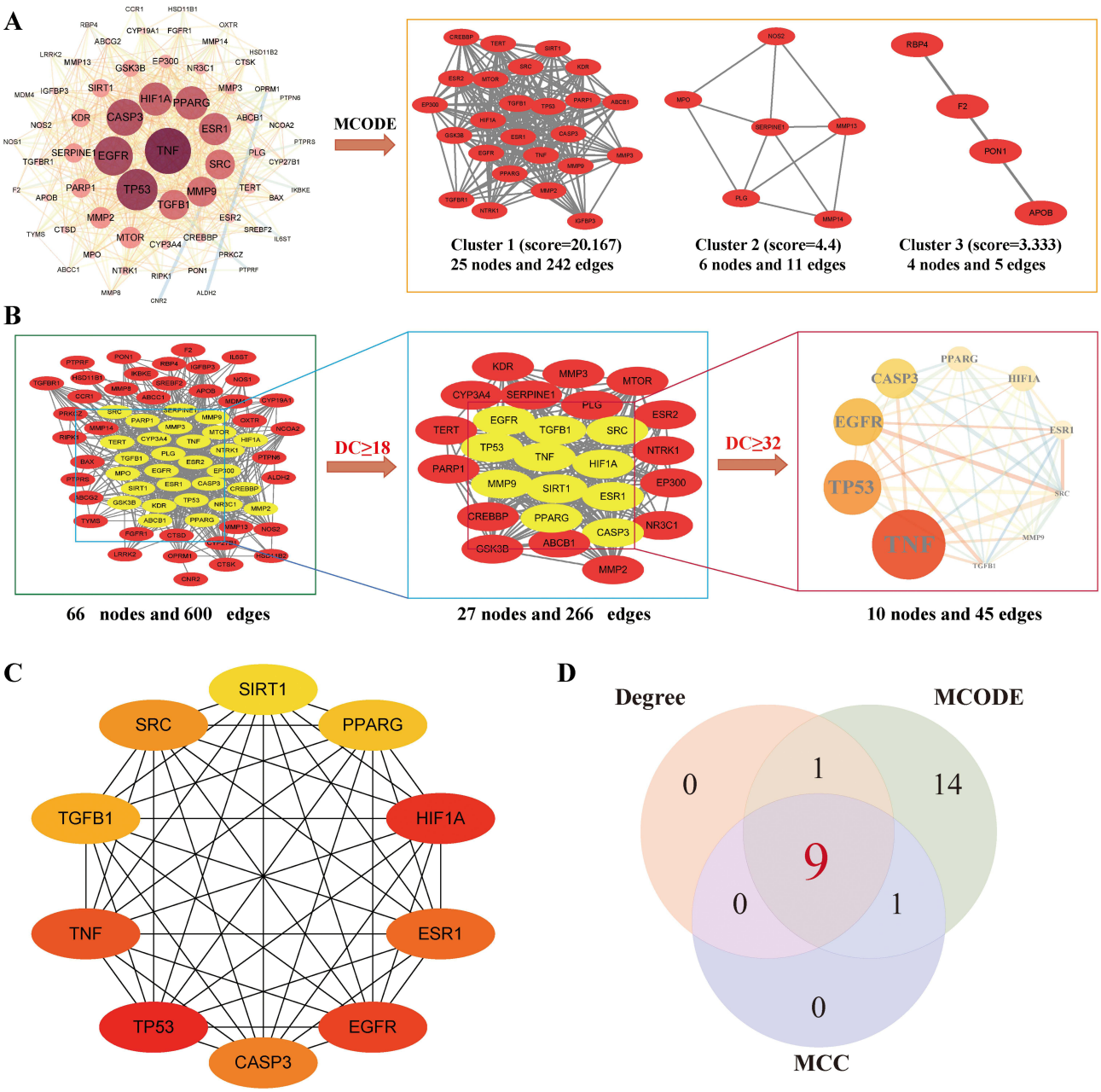

Figure 4 Identification of candidate targets via protein–protein interaction (PPI) analysis. (**A**) PPI network based on cluster analysis using the MCODE plug-in. (**B**) The process of topological screening for the PPI network. (**C**) The hub genes selected from the PPI network using the CytoHubba plugin. (**D**) The 9 core targets obtained by MCODE, topology analysis and MCC methods in the PPI network.

Molecular Dynamics Simulation

To assess the stability of protein-ligand complexes, molecular dynamics simulations were performed. Root mean square deviation (RMSD) serves as a robust metric for assessing the conformational stability of proteins and ligands. A smaller RMSD value indicates enhanced stability. As illustrated in Figure 9A, the PPARG-stigmasterol complex system of the small molecule and target protein achieved equilibrium after 5 ns, subsequently exhibiting fluctuations around 1.9 μM. This suggests that indicated that the conformation of the PPARG-stigmasterol protein-ligand complex remained in equilibrium, and the binding interaction was relatively stable Root mean square fluctuation (RMSF) provides insight into the flexibility of amino acid residues within the protein. As depicted in Figure 9B, the RMSF values for the PPARG-stigmasterol complex are relatively low, predominantly below 2 Å, suggesting low flexibility and high stability.

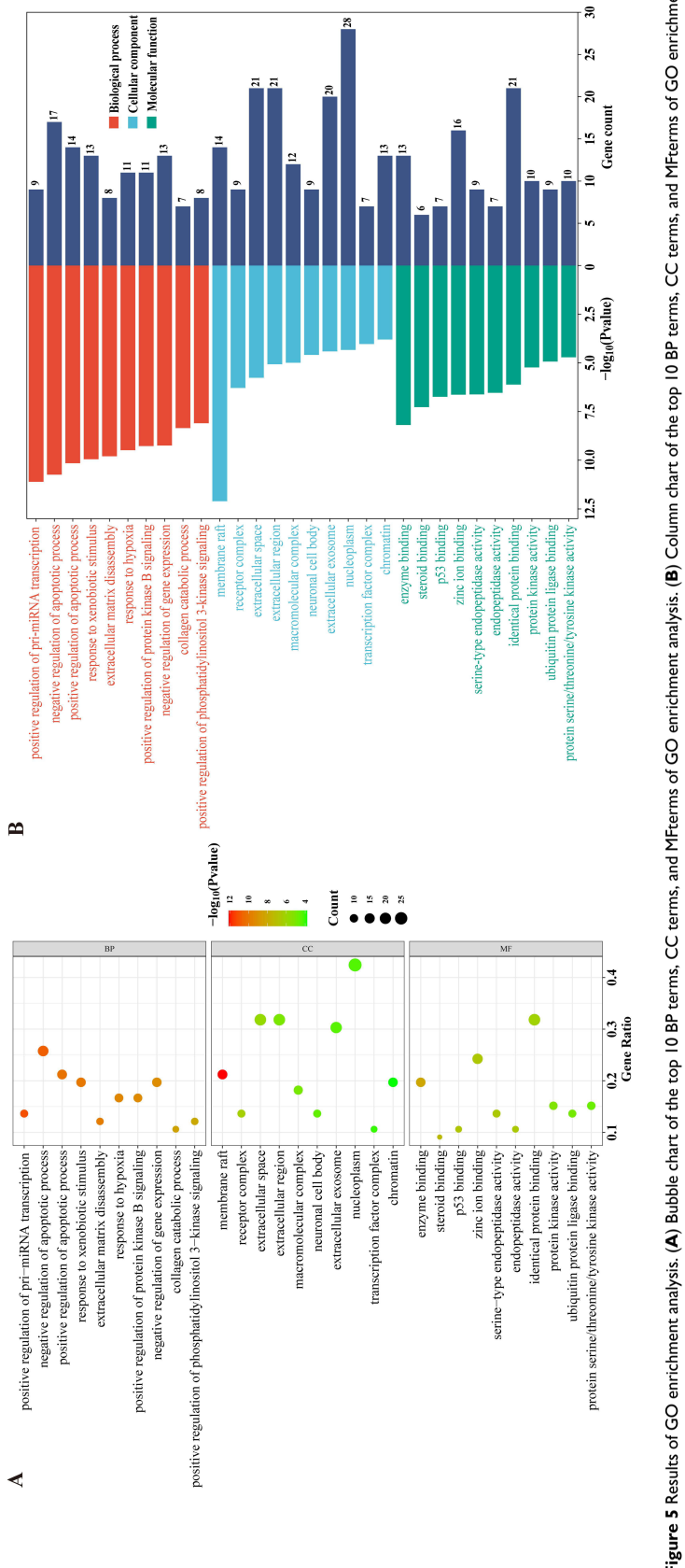

Figure 5 Results of GO enrichment analysis. (**A**) Bubble chart of the top 10 BP terms, CC terms, and MFterms of GO enrichment analysis. (**B**) Column chart of the top 10 BP terms, CC terms, and MFterms of GO enrichment analysis.

https://doi.org/10.2147/DDDT.S518115

Table 2 The KEGG Enrichment Results of the Top 20 Enriched Pathways

Pathway ID	Pathway Name	Count	Genes	*P*-value
hsa05200	Pathways in cancer	22	NTRK1, GSK3B, CREBBP, TGFB1, NOS2, MMP2, F2, HIF1A, ESR1, MMP9, EGFR, TGFBR1, MTOR, ESR2, TERT, CASP3, BAX, EP300, PPARG, IL6ST, TP53, FGFR1	2.94E-11
hsa05205	Proteoglycans in cancer	14	TGFB1, SRC, MMP2, HIF1A, ESR1, TNF, MMP9, EGFR, MTOR, CASP3, KDR, PTPN6, TP53, FGFR1	1.24E-09
hsa05167	Kaposi sarcoma-associated herpesvirus infection	12	CCR1, GSK3B, CREBBP, SRC, CASP3, EP300, BAX, IL6ST, HIF1A, TP53, IKBKE, MTOR	8.61E-08
hsa05161	Hepatitis B	11	CREBBP, TGFB1, SRC, CASP3, EP300, BAX, TNF, TP53, IKBKE, MMP9, TGFBR1	1.60E-07
hsa04926	Relaxin signaling pathway	10	TGFB1, MMP13, NOS2, SRC, MMP2, NOS1, PRKCZ, MMP9, EGFR, TGFBR1	2.50E-07
hsa05215	Prostate cancer	9	GSK3B, CREBBP, MMP3, EP300, TP53, MMP9, EGFR, MTOR, FGFR1	3.39E-07
hsa01522	Endocrine resistance	9	SRC, MMP2, BAX, ESR1, TP53, MMP9, EGFR, ESR2, MTOR	3.67E-07
hsa04919	Thyroid hormone signaling pathway	9	NCOA2, GSK3B, CREBBP, SRC, EP300, HIF1A, ESR1, TP53, MTOR	1.85E-06
hsa05210	Colorectal cancer	8	GSK3B, TGFB1, CASP3, BAX, TP53, EGFR, TGFBR1, MTOR	2.13E-06
hsa05417	Lipid and atherosclerosis	11	GSK3B, SRC, CASP3, MMP3, BAX, PPARG, APOB, TNF, TP53, IKBKE, MMP9	2.19E-06
hsa04520	Adherens junction	8	CREBBP, SRC, EP300, PTPN6, PTPRF, EGFR, TGFBR1, FGFR1	3.61E-06
hsa05152	Tuberculosis	10	CREBBP, TGFB1, NOS2, SRC, VDR, CASP3, EP300, BAX, TNF, CTSD	4.12E-06
hsa04210	Apoptosis	9	NTRK1, PARP1, CASP3, CTSK, BAX, RIPK1, TNF, CTSD, TP53	4.46E-06
hsa04915	Estrogen signaling pathway	9	NCOA2, SRC, MMP2, OPRM1, ESR1, CTSD, MMP9, EGFR, ESR2	4.71E-06
hsa04933	AGE-RAGE signaling pathway in diabetic complications	8	TGFB1, CASP3, MMP2, SERPINE1, BAX, TNF, PRKCZ, TGFBR1	5.87E-06
hsa05226	Gastric cancer	9	GSK3B, TGFB1, ABCB1, TERT, BAX, TP53, EGFR, TGFBR1, MTOR	8.78E-06
hsa05165	Human papillomavirus infection	12	GSK3B, CREBBP, TERT, CASP3, EP300, BAX, TNF, TP53, PRKCZ, IKBKE, EGFR, MTOR	1.65E-05
hsa05163	Human cytomegalovirus infection	10	CCR1, GSK3B, SRC, CASP3, BAX, RIPK1, TNF, TP53, EGFR, MTOR	2.50E-05
hsa04657	IL-17 signaling pathway	7	GSK3B, MMP13, CASP3, MMP3, TNF, IKBKE, MMP9	4.83E-05
hsa05206	MicroRNAs in cancer	11	ABCC1, CREBBP, ABCB1, CASP3, EP300, MDM4, SIRT1, TP53, MMP9, EGFR, MTOR	5.40E-05

Hydrogen bonds are crucial in facilitating ligand-protein interactions. Figure 9C shows that that the number of hydrogen bonds within the PPARG-stigmasterol complex ranges from 0 to 2, with one hydrogen bond being most prevalent. This pattern suggests effective hydrogen bond interactions between the small molecule and the target protein. In summary, the PPARG-stigmasterol complex system exhibits strong and stable.

Animal Model Validation

SZY Decelerates the Development of SONFH

In order to further validate the predictions of the network pharmacology analysis, a SONFH-model mice were constructed and utilized to investigate the pharmacological mechanism of SZY in treating SONFH through in vivo animal experiments (Figure 10A). The histomorphometric analysis revealed distinct bone necrosis alterations in the SONFH group, including trabecular fractures, reduction, and thinning, as well as the presence of empty bone lacunae or dense nuclei of bone cells surrounded by necrotic bone marrow cells. Figure 10B illustrates that the incidence of empty bone lacunae was lower in the SZY treatment group compared to the SONFH group. These results suggest that compared to the control group, the SONFH model group exhibited a significant increase in the ratio of empty bone lacunae and the number of dense bone cell nuclei, with subsequent improvement (Figure 10C and D). Micro-CT imaging was utilized to

evaluate the microarchitecture of bone. The femoral heads' subchondral bone displayed a uniformly distributed and cohesive structure in the control group, in contrast to the SONFH group which exhibited notable damage to the subchondral trabeculae. Compared with the SONFH group, subsequent treatment with SZY resulted in significant improvement of the subchondral trabeculae (Figure 10E). Quantitative analysis of trabeculae revealed that BV/TV and Tb.Th were significantly increased in the SZY group compared to the SONFH group, while the Tb.Sp measurements in

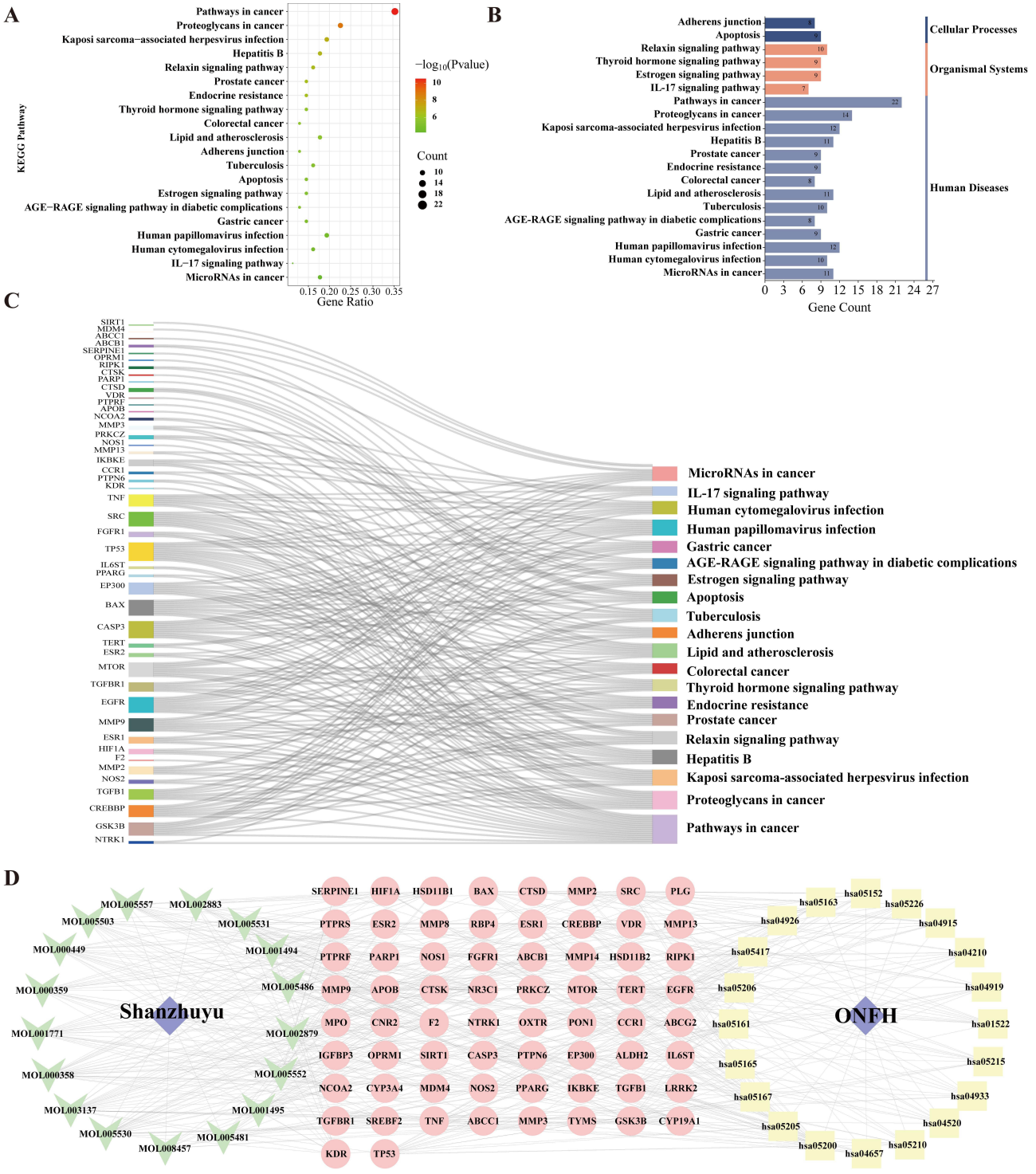

Figure 6 Continued.

https://doi.org/10.2147/DDDT.S518115

E

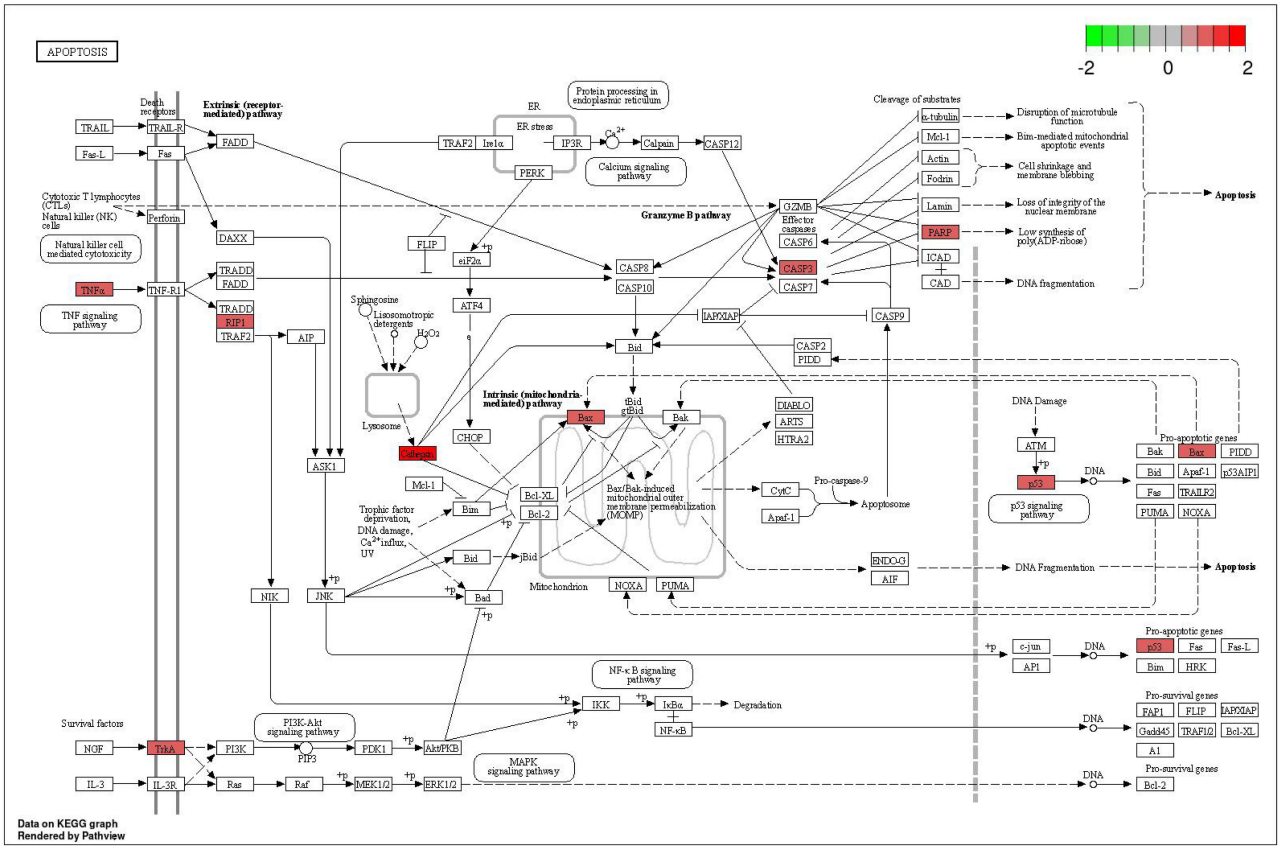

Figure 6 KEGG enrichment analysis for 66 common targets. (**A**) The bubble chart of the top 20 pathways based on KEGG enrichment analysis. (**B**) The KEGG type of the top 20 pathways based on KEGG enrichment analysis. (**C**) The Sankey diagram of the KEGG pathway analysis of the therapeutic targets of SZY in SONFH treatment. Distribution of key targets in the HIF-1 signaling pathway. (**D**) The Herb-Component-Target-Pathway network implicated in the mechanism of SZY in SONFH treatment. The pink nodes represent the targets; the yellow nodes represent the pathways, whereas the green nodes represent the compounds. (**E**) Distribution of key targets in the apoptosis signaling pathway. The red rectangle stands for the key targets.

the SZY group were significantly reduced (Figure 10F–H). These findings suggest that SZY treatment has a dose-dependent positive impact on bone health in SONFH mice, potentially reducing pathological injury in femoral heads and promoting osteoblast formation. SZY treatment can reduce the pathological injury in femoral heads in varying degrees and enhance osteoblast formation.

SZY Inhibited Inflammatory Reaction and Apoptosis of SONFH Mice

The results of the network pharmacology analysis indicate that SZY may exert osteoprotective effects through modulation of the apoptotic process. Immunohistochemical analysis demonstrated a significant upregulation of IL-6 and TNF-αexpression in the SONFH group, which was effectively attenuated by SZY treatment (Figure 11A). Quantitative analysis revealed a notable reduction in the expression of these proteins in the SZY group as compared to the SONFH group (Figure 11B and C). These results indicate that SZY possesses varying degrees of ability to inhibit the expression of inflammatory factors and alleviate inflammatory responses.

Additionally, the changes in the expression of apoptosis-related markers, specifically Caspase-3 and were validated via IF analysis (Figure 11D). The results of the analysis indicated a notable reduction in Bcl-2 expression and a substantial elevation in Caspase-3 expression in the femoral heads of SONFH mice compared to control mice. Notably, treatment with SZY effectively reversed these changes in Bcl-2 and Caspase-3 levels (Figure 11F and G). Furthermore, the process of apoptosis was validated through TUNEL staining. Our research demonstrated a significant increase in apoptosis within the femoral heads of SONFH mice, with SZY treatment showing a dose-dependent reduction

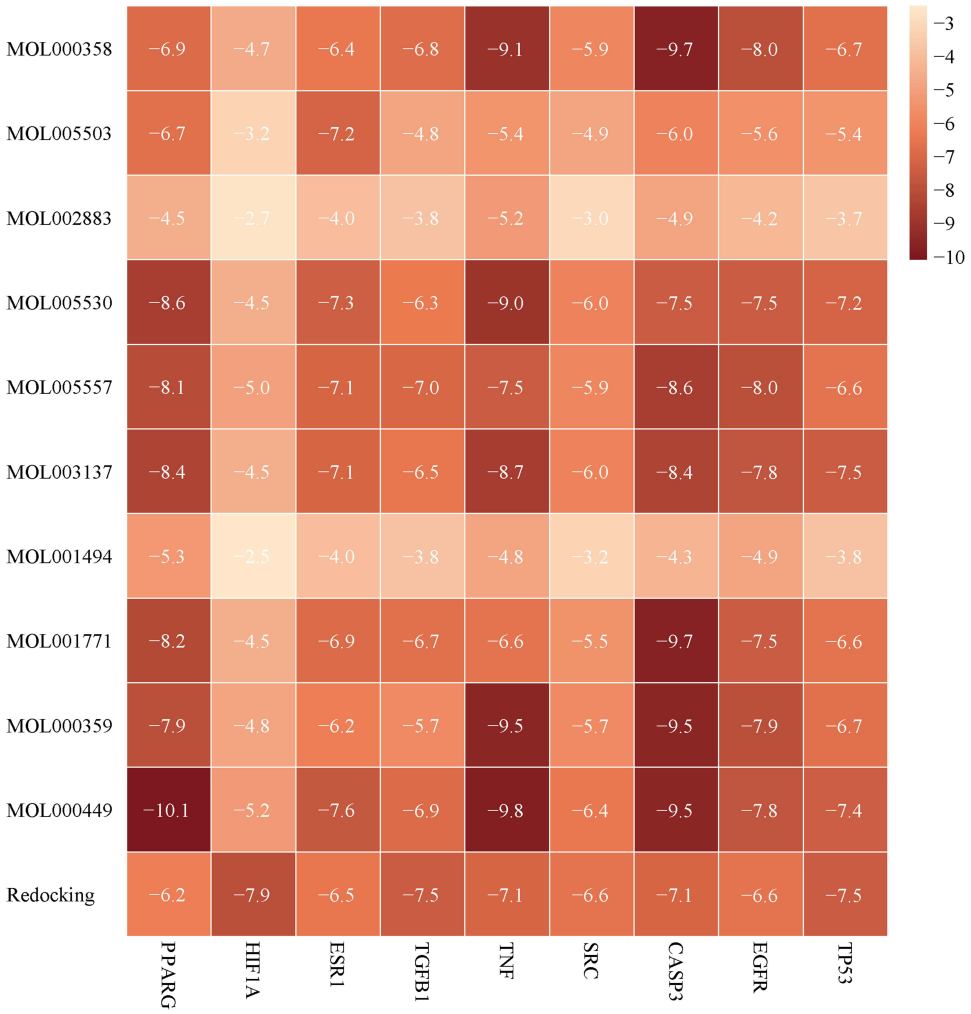

Figure 7 Heatmap of molecular docking score. Affinity energy (kcal/mol) of key targets and active compounds of herbs.

in apoptosis levels (Figure 11E and H). These findings indicate that SZY treatment inhibits the apoptosis process and mitigates the progression of SONFH by modulating apoptosis-related factors, including Bcl-2 and Caspase-3.

Discussion

SONFH is a degenerative skeletal condition characterized by femoral head collapse and hip joint dysfunction, necessitating total hip replacement surgery and significantly impacting both patient quality of life and global healthcare systems.[56,57] Bisphosphonates are FDA-approved effective drugs for the treatment of osteoporosis.[58] However, there is currently no effective drug for the treatment of SONFH in clinical practice, and many scholars are still exploring.[59] Traditional Chinese medicine has a long history of treating bone-related diseases and has shown good efficacy. SZY, a food with medicinal value, has demonstrated efficacy in treating bone-related diseases.[60] Currently, it has shown good efficacy in animal study, Nevertheless, the bioactive components and molecular mechanisms of SZY in the treatment of SONFH remain incompletely understood, hindering its advancement in modernization and internationalization, so we explored the potential therapeutic effect of SZY on SONFH. The innovative methodology of network pharmacology provides a systematic approach to understanding the mechanisms through which TCM influences various diseases.[61,62] This study aims to investigate the constituent components and pharmacological mechanisms underlying the therapeutic effects of SZY in the treatment of SONFH, employing a combination of network pharmacology analysis and experimental validation.

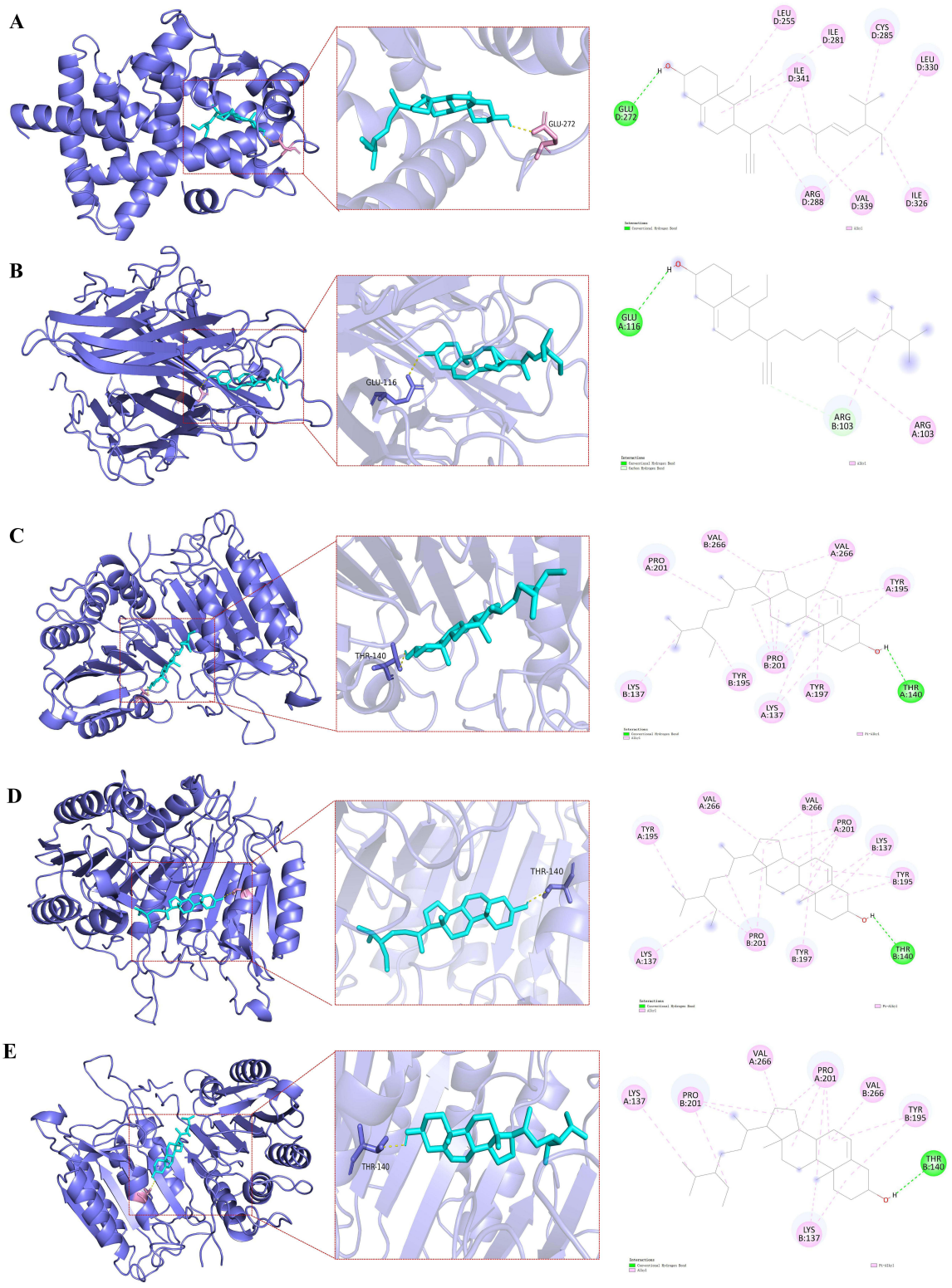

Figure 8 Continued.

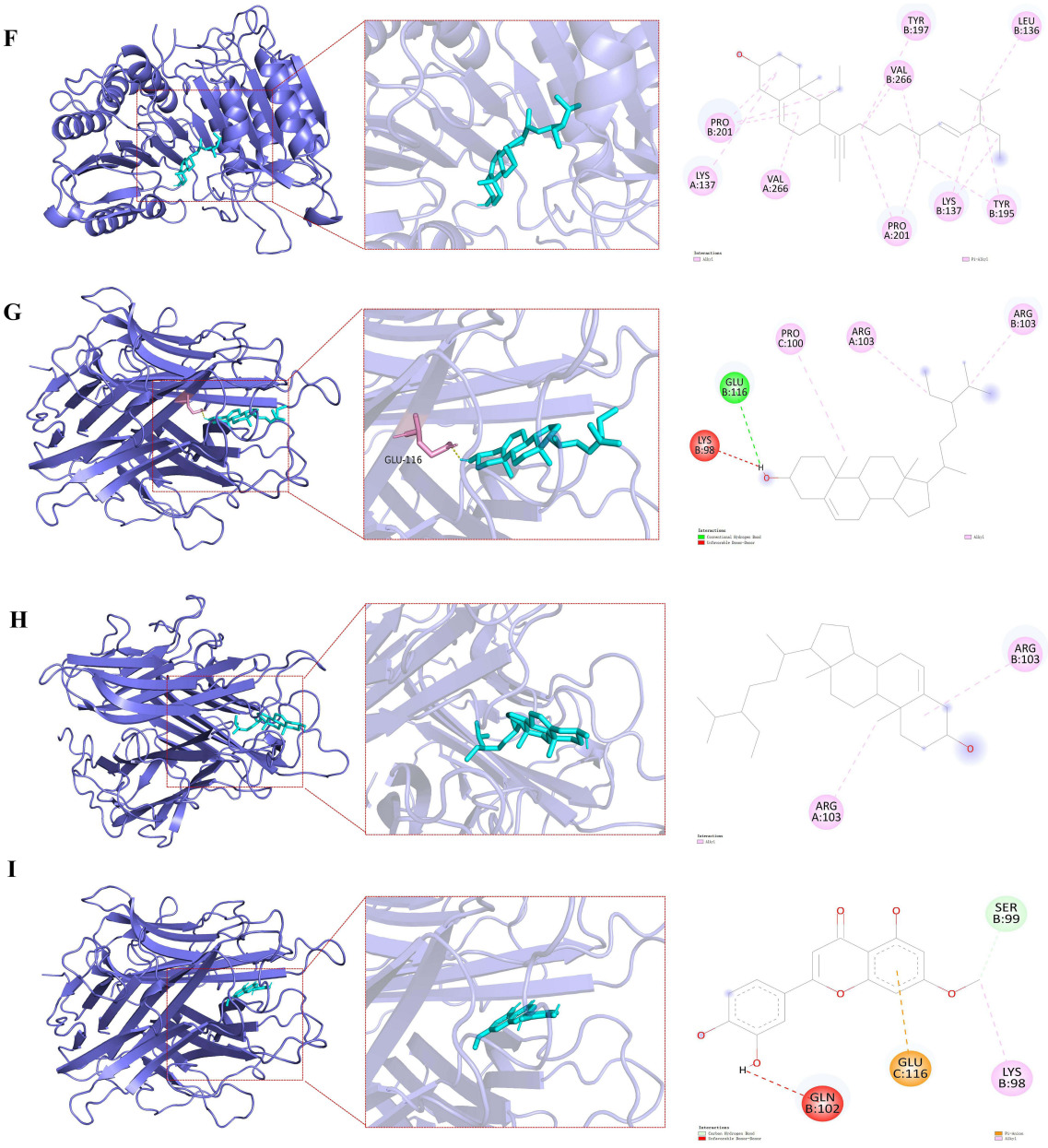

Figure 8 Docking modes between key targets and active compounds. (**A**) The binding modes of PPARG to Stigmasterol. (**B**) The binding modes of TNF to Stigmasterol. (**C**) The binding modes of CASP3 to beta-sitosterol. (**D**) The binding modes of CASP3 to poriferast-5-en-3beta-ol. (**E**) The binding modes of CASP3 to sitosterol. (**F**) The binding modes of CASP3 to Stigmasterol. (**G**) The binding modes of TNF to sitosterol. (**H**) The binding modes of TNF to beta-sitosterol. (**I**) The binding modes of TNF to Hydroxygenkwanin.

In the present study, twenty active components in SZY and 600 associated targets were identified. After constructing the component-target-pathway network, we identified the top 10 compounds including beta-sitosterol, cornudentanone, ethyloleate, hydroxygenkwanin, lanosta-8,24-dien-3-ol,3-acetate, leucanthoside, mandenolporiferast-5-en-3beta-ol, sitosterol, stigmasterol. Indeed, some component in SZY have been reported to show biological activities against bone-related diseases. For instance, beta-sitosterol has been shown to enhance bone length, weight, and mineral density, while also mitigating the elevation of bone resorption markers and the reduction of osteogenic markers. Beta-sitosterol demonstrates promise in mitigating glucocorticoid-induced osteoporosis through the protection of osteoblasts and inhibition of osteoclastogenesis. Prior studies have indicated that stigmasterol can impede the proliferation of fibroblast-like synoviocytes and facilitate their apoptosis.[63] Prior studies have shown that stigmasterol has the ability to impede the growth of

https://doi.org/10.2147/DDDT.S518115

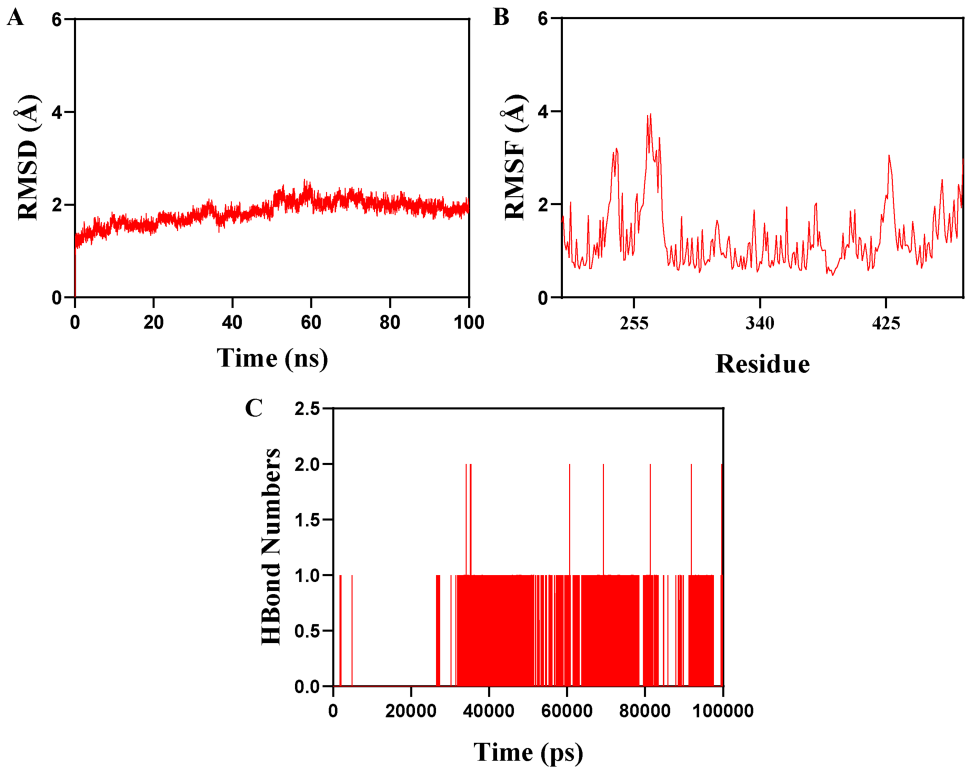

Figure 9 Molecular dynamics simulation of PPARG stigmasterol protein ligand complex. (**A**) The RMSD values of PPARG-stigmasterol complexes. (**B**)The RMSF values of PPARG-stigmasterol complexes. (**C**) The Hbonds values of PPARG-stigmasterol complexes.

fibroblast-like synoviocytes and induce apoptosis in these cells.[64] Consequently, these results suggest that various components within SZY may have significant therapeutic implications for the treatment of SONFH.

Based on topological analysis of the protein-protein interaction network, nine hub-targets were identified, including TNF, TP53, and CASP3, which are closely associated with inflammatory responses and apoptosis. TNF-α, a well-known proinflammatory cytokine, is recognized for its pivotal role in the development of SONFH. Prior research has indicated that the initiation of SONFH is influenced by TNF-α levels and a history of hypoxia.[65] TP53, a known apoptosis marker and transcription factor involved in cell cycle regulation, has been shown in a study to be regulated by Bre in osteoblast differentiation.[66] Downregulation of TP53 expression has been suggested as a potential protective measure against osteoporosis.[67] Additionally, Caspase-3, a key mediator of apoptosis, is capable of autonomously regulating cellular processes.[68] Prior research has indicated that erythropoietin (EPO) has demonstrated advantageous outcomes in rats afflicted with SANFH through the inhibition of STAT1-caspase 3 signaling.[69] Additionally, further investigations have validated the involvement of STAT1-mediated up-regulation of caspase-3 in osteoblast apoptosis induced by dexamethasone.[70] Collectively, these discoveries underscore the importance of TNF, TP53 and CASP3 in the apoptotic process and progression of SONFH.

Finally, molecular docking results verified that sitosterol, stigmasterol, and beta-sitosterol had better binding ability with CASP3 and TNF, further suggesting sitosterol, stigmasterol, and beta-sitosterol as promising drugs for the treatment of SONFH. These findings align with the outcomes of network pharmacology and animal studies. The results of molecular dynamics simulation also showed that PPARG-stigmasterol complex system showed good binding activity.

Furthermore, KEGG analysis suggested that SZY acts works synergistically on multiple sites and key pathways. Our study has also proved that the mechanism of SZY in treating SONFH is through regulating the expression of inflammatory factors and regulating apoptosis pathway, IL-17 signaling pathway and other signaling pathways. GO functional analysis and KEGG enrichment analyses highlighted the significant involvement of inflammatory response and apoptosis pathways in the biological processes and signaling pathways related to SONFH. Elevated inflammatory

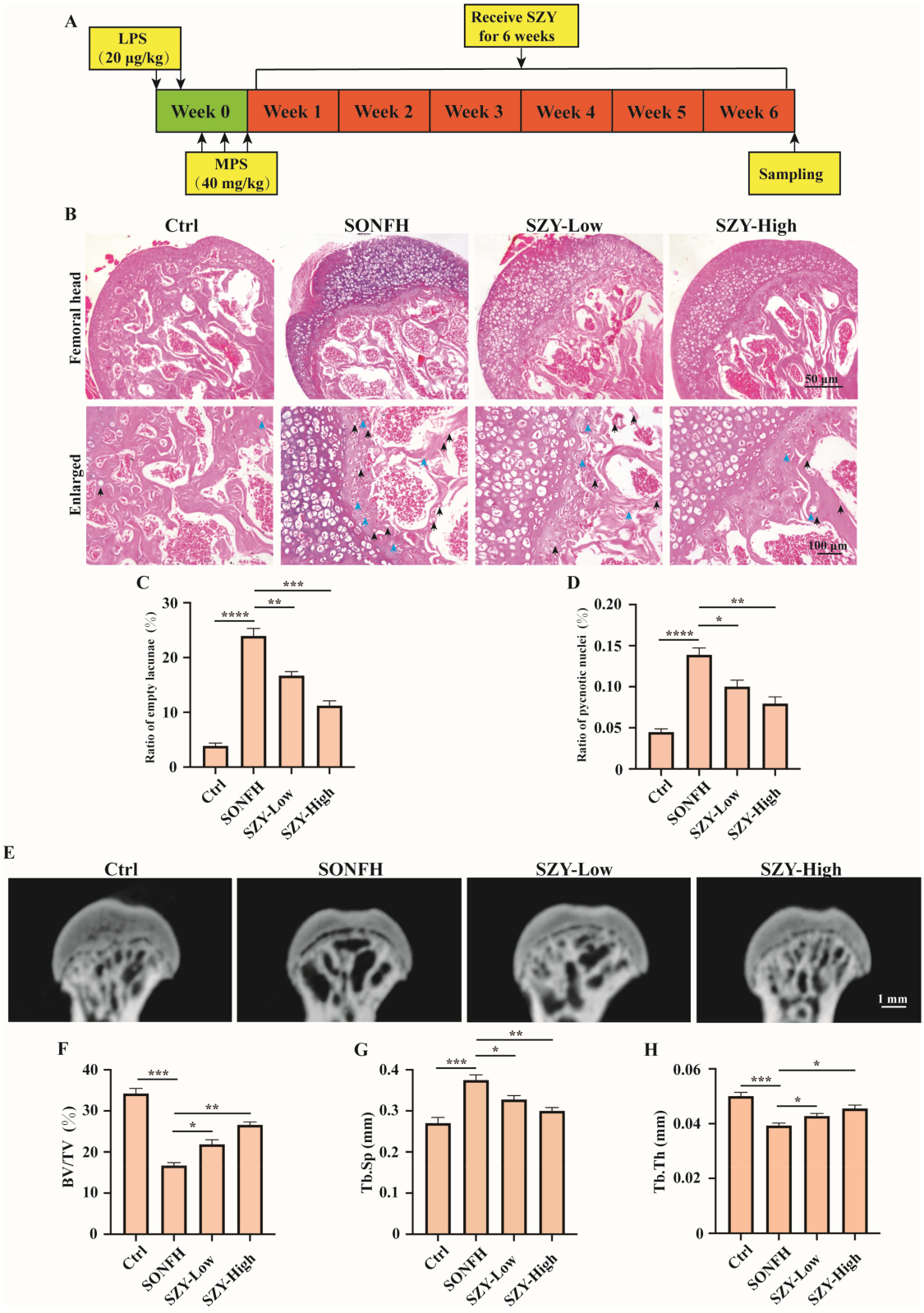

Figure 10 Histological features of mice femoral heads. (**A**) SONFH induction and treatment protocol. (**B**)Histological femoral head sections stained using Alcian blue/hematoxylin (ABH)/Orange G. The empty lacunae are indicated by black arrowheads; necrotic marrow cells are indicated by blue arrowheads. (**C**) The ratio of empty bone lacunae. (**D**) The number of nucleus pycnosis. (**E**) Representative micro-CT images. Quantification of the (**F**) BV/TV, (**G**) Tb. Sp and (**H**) Tb. Th by static histomorphometry. Data is expressed as mean±SD (n = 5). *P < 0.05 vs SONFH group, **P < 0.01 vs SONFH group, ***P < 0.001 vs SONFH group, ****P < 0.001 vs SONFH group.

https://doi.org/10.2147/DDDT.S518115

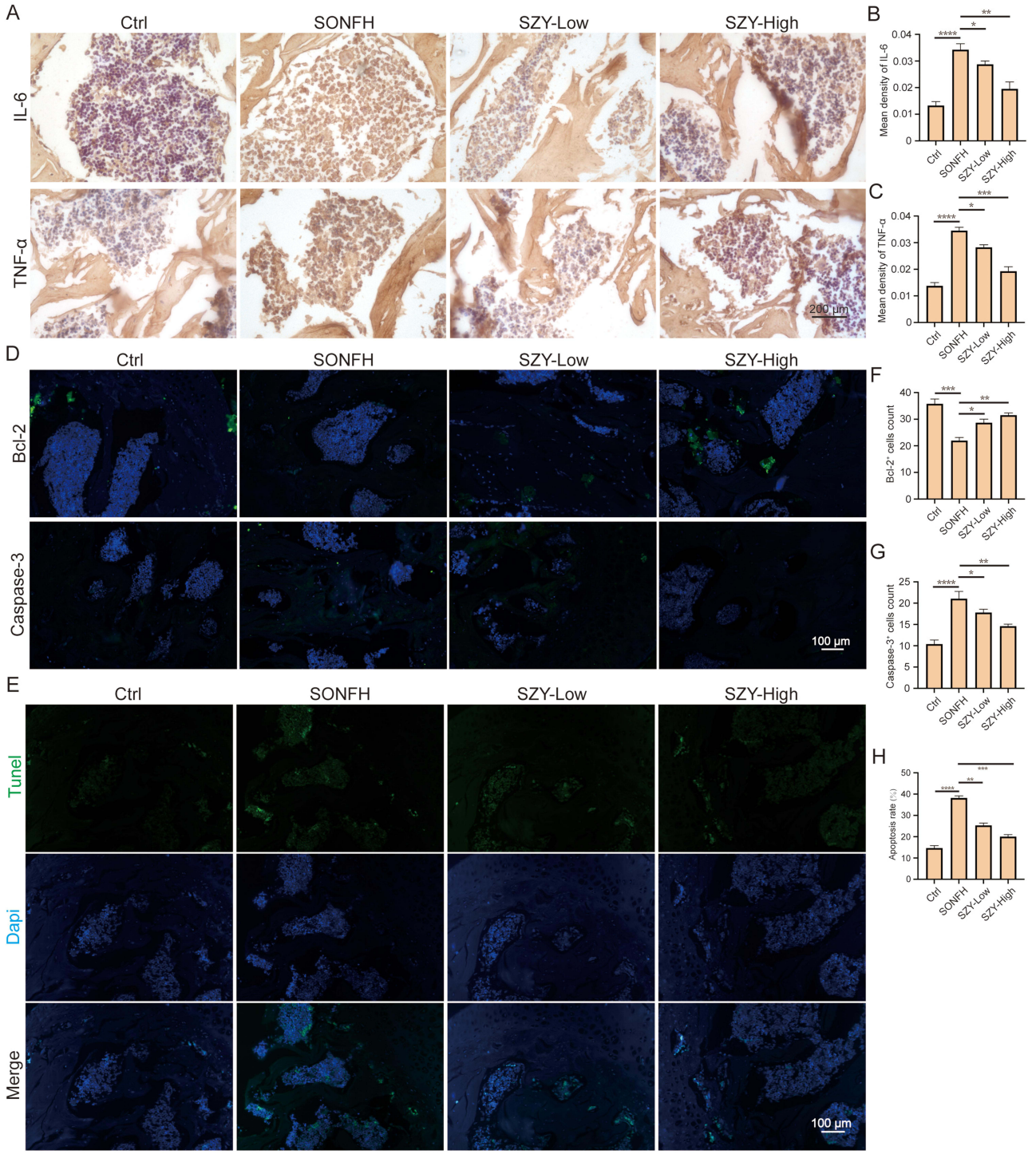

Figure 11 SZY inhibited inflammatory reaction and apoptosis of femoral heads to ameliorate SONFH. (**A**) Immunohistochemistry of IL-6 and TNF-αin femoral heads. (**B** and **C**) The quantification of IL-6 and TNF-αin femoral heads. (**D**) Immunofluorescence of Bcl-2 and Caspase-3 in femoral heads. (**E**) Tunel staining was used to detect the apoptosis of femoral heads. (**F** and **G**) The quantification of Bcl-2 and Caspase-3 positive cells in femoral heads. (**H**) The quantification of TUNEL positive rates in femoral heads. Scale bar = 100 μm. Data is expressed as mean±SD (n = 5). *P < 0.05 vs SONFH group, **P < 0.01 vs SONFH group, ***P < 0.001 vs SONFH group, ****P < 0.001 vs SONFH group.

response is a prominent characteristic of osteonecrosis of the femoral head. Studies have demonstrated that suppressing inflammatory responses can reduce the synthesis of pro-inflammatory cytokines, impede osteoclast differentiation, enhance bone regeneration, and alleviate ONFH.[71,72] Inflammatory response can promote the occurrence of cell apoptosis. Apoptosis, the principal mechanism of programmed cell death, plays a crucial role in maintaining bone

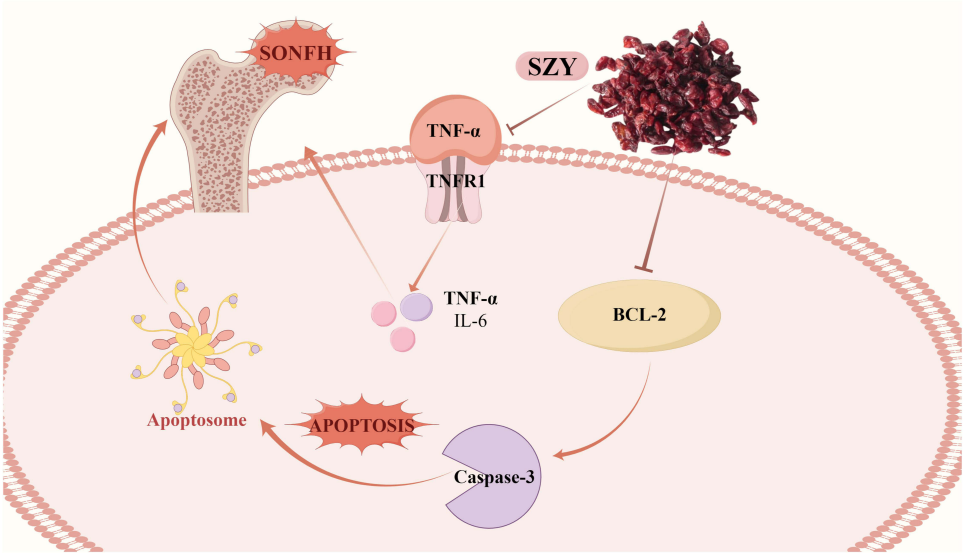

Figure 12 Schematic diagram of the potential mechanism by which SZY relieves SONFH via inhibiting apoptosis and inflammatory reaction.

homeostasis.[73] Multiple foundational studies have demonstrated the significant involvement of apoptosis in the physiological and pathological mechanisms of SONFH.[74,75] Subsequent in vivo animal experiments provided further evidence that SZY effectively suppressed apoptosis and inflammation in SONFH, thereby mitigating disease progression. The findings of our study suggest that SZY effectively reversed the dysregulated expression of key markers, including Bcl-2, Caspase-3, TNF, and IL-6, and decreased the elevated TUNEL positive rate in the femoral heads of mice with SONFH. These results provide insight into the potential therapeutic mechanisms of SZY in treating SONFH, which involve the modulation of apoptosis-related proteins and mitigation of inflammatory responses. SZY is a promising therapy for SONFH, which may offer an effective treatment for SONFH by targeting multiple ingredients, pathways, and targets simultaneously. Animal experiments confirmed that the protective effects of SZY against SONFH are likely mediated by the inhibition of inflammatory responses and apoptosis (Figure 12). While this study yielded significant preliminary results, it is crucial to acknowledge its limitations. Firstly, the predictions of this research mainly rely on databases and algorithms, and their results may differ from actual results. Moreover, the investigation primarily confirmed the essential role of inflammatory responses and the apoptosis pathway in the treatment of SONFH with SZY. Further validation is necessary to elucidate the relationships between the IL-17 signaling pathway, the estrogen signaling pathway, and other signaling pathways in the context of SONFH. Additionally, this study did not address the clinical safety of SZY in the treatment of SONFH, which may constrain the clinical application of SZY. Consequently, we intend to conduct more comprehensive in vitro and in vivo experiments to explore other potential mechanisms of action of SZY. We also plan to undertake single-center clinical studies to verify the safety and efficacy of SZY, thereby reinforcing its role in SONFH management and advancing the modernization of TCM.

Conclusion

In conclusion, this study utilized a range of methodologies, including network pharmacology, molecular docking, and in vivo experimental validation, to investigate the therapeutic potential of SZY in the treatment of SONFH. This integrative approach bridges the holistic principles of TCM with modern systems biology, offering a replicable framework for the examination of other herbal therapies. Our findings suggest that SZY therapy for SONFH operates through multi-component, multi-target, and multi-pathway mechanisms. The primary pathways involved in the regulation of SONFH include the apoptosis pathway, the IL-17 signaling pathway, among others. Further in vivo experiments have demonstrated that SZY exerts its effects on SONFH by inhibiting inflammatory responses and cell apoptosis. Nevertheless, additional in vitro and clinical studies are necessary to fully elucidate its function and safety profile. Overall, this study not only provides a theoretical foundation and experimental data for the pharmacological properties and potential

https://doi.org/10.2147/DDDT.S518115

mechanisms of SZY in SONFH treatment, but also offers guidance for the clinical application and future research priorities of SZY.

Acknowledgments

This work was supported by the National Natural Science Foundation of China (No. 82205136), Zhejiang Traditional Chinese Medicine Administration (No. 2025ZL099, No. 2017ZKL017, No. 2022ZA129, No. 2020ZB191), Hangzhou Biomedical and Health Industry Development Support Technology Special Project (No.2021WJCY176), Hangzhou Science and Technology Bureau (20201203B222).

Disclosure

The authors declare no conflicts of interest in this work.

References

1. Chen K, Liu Y, He J, et al. Steroid-induced osteonecrosis of the femoral head reveals enhanced reactive oxygen species and hyperactive osteoclasts. *Int J Bio Sci*. 2020;16(11):1888–1900. doi:10.7150/ijbs.40917
2. Liu N, Zheng C, Wang Q, Huang Z. Treatment of non-traumatic avascular necrosis of the femoral head (Review). *Exp Ther Med*. 2022;23(5):321. doi:10.3892/etm.2022.11250
3. Kubo T, Fujioka M, Ishida M. Clinical condition of steroid-induced osteonecrosis of the femoral head. *Clin Calcium*. 2007;17(6):856–862.
4. Kubo T, Ueshima K, Saito M, Ishida M, Arai Y, Fujiwara H. Clinical and basic research on steroid-induced osteonecrosis of the femoral head in Japan. *J Orthopaedic Sci*. 2016;21(4):407–413. doi:10.1016/j.jos.2016.03.008
5. Wu H, Cheng K, Tong L, Wang Y, Yang W, Sun Z. Knowledge structure and emerging trends on osteonecrosis of the femoral head: a bibliometric and visualized study. *J Orthopaedic Surg Res*. 2022;17(1):194. doi:10.1186/s13018-022-03068-7
6. Chang C, Greenspan A, Gershwin ME. The pathogenesis, diagnosis and clinical manifestations of steroid-induced osteonecrosis. *J Autoimmun*. 2020;110:102460. doi:10.1016/j.jaut.2020.102460
7. Luo D, Gao X, Zhu X, et al. Identification of steroid-induced osteonecrosis of the femoral head biomarkers based on immunization and animal experiments. *BMC Musculoskeletal Disorders*. 2024;25(1):596. doi:10.1186/s12891-024-07707-4
8. Zhang X, Yang Z, Xu Q, et al. Dexamethasone induced osteocyte apoptosis in steroid-induced femoral head osteonecrosis through ROS-mediated oxidative stress. *Orthopaedic Surg*. 2024;16(3):733–744. doi:10.1111/os.14010
9. Jia D, Zhang Y, Li H, et al. Predicting steroid-induced osteonecrosis of the femoral head: role of lipid metabolism biomarkers and radiomics in young and middle-aged adults. *J Orthopaedic Surg Res*. 2024;19(1):749. doi:10.1186/s13018-024-05245-2
10. Lu C, Qi H, Xu H, et al. Global research trends of steroid-induced osteonecrosis of the femoral head: a 30-year bibliometric analysis. *Front Endocrinol*. 2022;13:1027603. doi:10.3389/fendo.2022.1027603
11. Fu W, Liu B, Wang B, Zhao D. Early diagnosis and treatment of steroid-induced osteonecrosis of the femoral head. *Int Orthopaedics*. 2019;43(5):1083–1087. doi:10.1007/s00264-018-4011-y
12. Li XH, Qian SD, Chen D, et al. A new mechanism in steroid-induced osteonecrosis of the femoral head and the protective role of simvastatin. *Exp Cell Res*. 2025;446(1):114471. doi:10.1016/j.yexcr.2025.114471
13. Zhu K, Liu W, Peng Y, et al. Study on the mechanism of Shuanghe decoction against steroid-induced osteonecrosis of the femoral head: insights from network pharmacology, metabolomics, and gut microbiota. *J Orthopaedic Surg Res*. 2025;20(1):202. doi:10.1186/s13018-025-05619-0
14. Tang X, Huang Y, Fang X, et al. *Cornus officinalis*: a potential herb for treatment of osteoporosis. *Front Med*. 2023;10:1289144. doi:10.3389/fmed.2023.1289144
15. Chen R, Song C, Qiu J, et al. Exploring the potential mechanism of Taohong Siwu decoction in the treatment of avascular necrosis of the femoral head based on network pharmacology and molecular docking. *Medicine*. 2023;102(50):e35312. doi:10.1097/md.0000000000035312
16. Li H, Zhang Y, Hao Y, et al. Proanthocyanidins inhibit osteoblast apoptosis via the PI3K/AKT/Bcl-xL pathway in the treatment of steroid-induced osteonecrosis of the femoral head in rats. *Nutrients*. 2023;15(8). doi:10.3390/nu15081936
17. Ren GW, Wen SB, Han J, et al. Network-based pharmacology and bioinformatics study on the mechanism of action of gujiansan in the treatment of steroid-induced avascular necrosis of the femoral head. *Biomed Res Int*. 2022;2022:8080679. doi:10.1155/2022/8080679
18. Deng W, Liu Y, Guo Y, et al. A comprehensive review of *Cornus officinalis*: health benefits, phytochemistry, and pharmacological effects for functional drug and food development. *Front Nutr*. 2023;10:1309963. doi:10.3389/fnut.2023.1309963
19. Gao X, Liu Y, An Z, Ni J. Active components and pharmacological effects of Cornus *officinalis*: literature review. *Front Pharmacol*. 2021;12:633447. doi:10.3389/fphar.2021.633447
20. Kim JY, Kim YK, Choi MK, Oh J, Kwak HB, Kim JJ. Effect of Cornus *officinalis* on receptor activator of nuclear factor-kappaB Ligand (RANKL)-induced osteoclast differentiation. *J Bone Metabol*. 2012;19(2):121–127. doi:10.11005/jbm.2012.19.2.121
21. Park E, Lee CG, Kim J, et al. Anti-osteoporotic effects of the herbal mixture of Cornus *officinalis* and achyranthes japonica in vitro and in vivo. *Plants*. 2020;9(9). doi:10.3390/plants9091114
22. Zhao L, Zhang H, Li N, et al. Network pharmacology, a promising approach to reveal the pharmacology mechanism of Chinese medicine formula. *J Ethnopharmacol*. 2023;309:116306. doi:10.1016/j.jep.2023.116306
23. Li X, Liu Z, Liao J, Chen Q, Lu X, Fan X. Network pharmacology approaches for research of traditional Chinese medicines. *Chinese J Nat Med*. 2023;21(5):323–332. doi:10.1016/s1875-5364(23)60429-7
24. Jiashuo WU, Fangqing Z, Zhuangzhuang LI, Weiyi J, Yue S. Integration strategy of network pharmacology in Traditional Chinese Medicine: a narrative review. *Journal of Traditional Chinese Medicine = Chung I Tsa Chih Ying Wen Pan*. 2022;42(3):479–486. doi:10.19852/j.cnki.jtcm.20220408.003

25. Zhang P, Zhang D, Zhou W, et al. Network pharmacology: towards the artificial intelligence-based precision traditional Chinese medicine. *Briefings Bioinf*. 2023;25:1. doi:10.1093/bib/bbad518
26. Ru J, Li P, Wang J, et al. TCMSP: a database of systems pharmacology for drug discovery from herbal medicines. *J Cheminf*. 2014;6:13. doi:10.1186/1758-2946-6-13
27. van der Graaf PH, Benson N. Systems pharmacology: bridging systems biology and pharmacokinetics-pharmacodynamics (PKPD) in drug discovery and development. *Pharm Res*. 2011;28(7):1460–1464. doi:10.1007/s11095-011-0467-9
28. Bateman A, Martin M-J, Orchard S. UniProt: the Universal Protein Knowledgebase in 2023. *Nucleic Acids Res*. 2023;51(D1):D523–d531. doi:10.1093/nar/gkac1052
29. Gfeller D, Grosdidier A, Wirth M, Daina A, Michielin O, Zoete V. SwissTargetPrediction: a web server for target prediction of bioactive small molecules. *Nucleic Acids Res*. 2014;42(Web Server issue):W32–8. doi:10.1093/nar/gku293
30. Rebhan M, Chalifa-Caspi V, Prilusky J, Lancet D. GeneCards: integrating information about genes, proteins and diseases. *Trends Genet*. 1997;13 (4):163. doi:10.1016/s0168-9525(97)01103-7
31. Amberger JS, Bocchini CA, Schiettecatte F, Scott AF, Hamosh A. OMIM.org: online Mendelian inheritance in man (OMIM®), an online catalog of human genes and genetic disorders. *Nucleic Acids Res*. 2015;43(Database issue):D789–98. doi:10.1093/nar/gku1205
32. Piñero J, Ramírez-Anguita JM, Saüch-Pitarch J, et al. The DisGeNET knowledge platform for disease genomics: 2019 update. *Nucleic Acids Res*. 2020;48(D1):D845–d855. doi:10.1093/nar/gkz1021
33. Knox C, Wilson M, Klinger CM, et al. DrugBank 6.0: the DrugBank Knowledgebase for 2024. *Nucleic Acids Res*. 2024;52(D1):D1265–d1275. doi:10.1093/nar/gkad976
34. Sayers EW, Bolton EE, Brister JR, et al. Database resources of the national center for biotechnology information. *Nucleic Acids Res*. 2022;50(D1): D20–d26. doi:10.1093/nar/gkab1112
35. Szklarczyk D, Morris JH, Cook H, et al. The STRING database in 2017: quality-controlled protein-protein association networks, made broadly accessible. *Nucleic Acids Res*. 2017;45(D1):D362–d368. doi:10.1093/nar/gkw937
36. Shannon P, Markiel A, Ozier O, et al. Cytoscape: a software environment for integrated models of biomolecular interaction networks. *Genome Res*. 2003;13(11):2498–2504. doi:10.1101/gr.1239303
37. Zhang R, Guo H, Yang X, et al. Pathway-based network analyses and candidate genes associated with Kashin-Beck disease. *Medicine*. 2019;98 (18):e15498. doi:10.1097/md.0000000000015498
38. Chin CH, Chen SH, Wu HH, Ho CW, Ko MT, Lin CY. cytoHubba: identifying hub objects and sub-networks from complex interactome. *BMC Syst Biol*. 2014;8 Suppl 4(Suppl 4):S11. doi:10.1186/1752-0509-8-s4-s11
39. Gu S, Xue Y, Gao Y, et al. Mechanisms of indigo naturalis on treating ulcerative colitis explored by GEO gene chips combined with network pharmacology and molecular docking. *Sci Rep*. 2020;10(1):15204. doi:10.1038/s41598-020-71030-w
40. Kim S, Thiessen PA, Bolton EE, et al. PubChem substance and compound databases. *Nucleic Acids Res*. 2016;44(D1):D1202–13. doi:10.1093/nar/gkv951
41. Berman HM, Westbrook J, Feng Z, et al. The protein data bank. *Nucleic Acids Res*. 2000;28(1):235–242. doi:10.1093/nar/28.1.235
42. Trott O, Olson AJ. AutoDock Vina: improving the speed and accuracy of docking with a new scoring function, efficient optimization, and multithreading. *J Comput Chem*. 2010;31(2):455–461. doi:10.1002/jcc.21334
43. Zhang X, Yang Y, Wen M, et al. Supplementary hesperidin alleviated CPT-11-induced diarrhea by modulating gut microbiota and inhibiting the IL-17 signaling pathway. *J Agri Food Chem*. 2025;73(10):5915–5930. doi:10.1021/acs.jafc.4c09602
44. Khare SC, Gupta S T, Patel A, Patel A. Analyzing phytocompounds, antioxidants, and in-silico molecular docking of plant-derived potential andrographis paniculata inhibitory action to managed beta thalassemia. *Medin*. 2024;1(3):122–130. doi:10.47852/bonviewMEDIN42021979
45. Ajayi IIF TH, Alonge AS, Saliu IO, Odesanmi OE, Akinyelu J, Oke OE. ADME, molecular targets, docking, and dynamic simulation studies of phytoconstituents of Cymbopogon *citratus* (DC.). *Medin*. 2024;1(3):152–163. doi:10.47852/bonviewMEDIN42022711
46. AlRawashdeh S, Barakat KH. Applications of molecular dynamics simulations in drug discovery. *Methods Mol Biol*. 2024;2714:127–141. doi:10.1007/978-1-0716-3441-7_7
47. Jo S, Kim T, Iyer VG, Im W. CHARMM-GUI: a web-based graphical user interface for CHARMM. *J Comput Chem*. 2008;29(11):1859–1865. doi:10.1002/jcc.20945
48. Lohachova KO, Kyrychenko A, Kalugin ON. Critical assessment of popular biomolecular force fields for molecular dynamics simulations of folding and enzymatic activity of main protease of coronavirus SARS-CoV-2. *Biophys Chem*. 2024;311:107258. doi:10.1016/j.bpc.2024.107258
49. Filipe HAL, Loura LMS. Molecular dynamics simulations: advances and applications. *Molecules*. 2022;27(7):2105. doi:10.3390/molecules27072105
50. Qin L, Zhang G, Sheng H, et al. Multiple bioimaging modalities in evaluation of an experimental osteonecrosis induced by a combination of lipopolysaccharide and methylprednisolone. *Bone*. 2006;39(4):863–871. doi:10.1016/j.bone.2006.04.018
51. Zhang P, Xu H, Wang P, et al. Yougui pills exert osteoprotective effects on rabbit steroid-related osteonecrosis of the femoral head by activating β-catenin. *Biomed Pharmacothe*. 2019;120:109520. doi:10.1016/j.biopha.2019.109520
52. Yamamoto T, Irisa T, Sugioka Y, Sueishi K. Effects of pulse methylprednisolone on bone and marrow tissues: corticosteroid-induced osteonecrosis in rabbits. *Arthritis Rheum*. 1997;40(11):2055–2064. doi:10.1002/art.1780401119
53. Wu X, Pang L, Lei W, et al. Inhibition of Sca-1-positive skeletal stem cell recruitment by alendronate blunts the anabolic effects of parathyroid hormone on bone remodeling. *Cell Stem Cell*. 2010;7(5):571–580. doi:10.1016/j.stem.2010.09.012
54. Fu F, Bao R, Yao S, et al. Aberrant spinal mechanical loading stress triggers intervertebral disc degeneration by inducing pyroptosis and nerve ingrowth. *Sci Rep*. 2021;11(1):772. doi:10.1038/s41598-020-80756-6
55. Zhang H, Yao S, Zhang Z, et al. Network pharmacology and experimental validation to reveal the pharmacological mechanisms of liuwei dihuang decoction against intervertebral disc degeneration. *Drug Des Devel Ther*. 2021;15:4911–4924. doi:10.2147/dddt.S338439
56. Motta F, Timilsina S, Gershwin ME, Selmi C. Steroid-induced osteonecrosis. *J Trans Autoimmun*. 2022;5:100168. doi:10.1016/j.jtauto.2022.100168
57. Huang C, Wen Z, Niu J, Lin S, Wang W. Steroid-induced osteonecrosis of the femoral head: novel insight into the roles of bone endothelial cells in pathogenesis and treatment. *Front Cell Develop Biol*. 2021;9:777697. doi:10.3389/fcell.2021.777697

58. Gehrke B, Alves Coelho MC, Brasil d'Alva C, Madeira M. Long-term consequences of osteoporosis therapy with bisphosphonates. *Arch Endocrinol Metabol*. 2023;68:e220334. doi:10.20945/2359-4292-2022-0334
59. Fan Y, Chen Z, Wang H, et al. Isovitexin targets SIRT3 to prevent steroid-induced osteonecrosis of the femoral head by modulating mitophagy-mediated ferroptosis. *Bone Res*. 2025;13(1):18. doi:10.1038/s41413-024-00390-0
60. Ma W, Wang KJ, Cheng CS, et al. Bioactive compounds from *Cornus officinalis* fruits and their effects on diabetic nephropathy. *J Ethnopharmacol*. 2014;153(3):840–845. doi:10.1016/j.jep.2014.03.051
61. Li X, Wei S, Niu S, et al. Network pharmacology prediction and molecular docking-based strategy to explore the potential mechanism of Huanglian Jiedu Decoction against sepsis. *Comput Biol Med*. 2022;144:105389. doi:10.1016/j.compbiomed.2022.105389
62. Shang L, Wang Y, Li J, et al. Mechanism of Sijunzi Decoction in the treatment of colorectal cancer based on network pharmacology and experimental validation. *J Ethnopharmacol*. 2023;302(Pt A):115876. doi:10.1016/j.jep.2022.115876
63. Wang T, Li S, Yi C, Wang X, Han X. Protective role of β-sitosterol in glucocorticoid-induced osteoporosis in rats via the RANKL/OPG pathway. *Alternative Therap Health Med*. 2022;28(7):18–25.
64. Yao X, Hou L, Xia C, et al. Stigmasterol depresses the proliferation and facilitates the apoptosis of fibroblast-like synoviocytes via the PI3K/AKT signaling pathway in collagen-induced arthritis rats. *Alternative Therap Health Med*. 2023;29:644–649.
65. Liu Y, Jiang W, Liu S, Su X, Zhou S. Combined effect of tnf-α polymorphisms and hypoxia on steroid-induced osteonecrosis of femoral head. *Int J Clin Exp Pathol*. 2015;8(3):3215–3219.
66. Jin F, Wang Y, Wang X, et al. Bre enhances osteoblastic differentiation by promoting the Mdm2-mediated degradation of p53. *Stem Cells*. 2017;35(7):1760–1772. doi:10.1002/stem.2620
67. Yu T, Wu Q, You X, et al. Tomatidine alleviates osteoporosis by downregulation of p53. *Med Sci Monitor*. 2020;26:e923996. doi:10.12659/msm.923996
68. Porter AG, Jänicke RU. Emerging roles of caspase-3 in apoptosis. *Cell Death Differ*. 1999;6(2):99–104. doi:10.1038/sj.cdd.4400476
69. Cai T, Chen S, Wu C, et al. Erythropoietin suppresses osteoblast apoptosis and ameliorates steroid-induced necrosis of the femoral head in rats by inhibition of STAT1-caspase 3 signaling pathway. *BMC Musculoskeletal Disorders*. 2023;24(1):894. doi:10.1186/s12891-023-07028-y
70. Feng Z, Zheng W, Tang Q, et al. Fludarabine inhibits STAT1-mediated up-regulation of caspase-3 expression in dexamethasone-induced osteoblasts apoptosis and slows the progression of steroid-induced avascular necrosis of the femoral head in rats. *Apoptosis*. 2017;22(8):1001–1012. doi:10.1007/s10495-017-1383-1
71. Kim HKW, Park MS, Alves Do Monte F, Gokani V, Aruwajoye OO, Ren Y. Minimally invasive necrotic bone washing improves bone healing after femoral head ischemic osteonecrosis: an experimental investigation in immature pigs. *J Bone Joint Surg Am Vol*. 2021;103(13):1193–1202. doi:10.2106/jbjs.20.00578
72. Wang M, Min HS, Shan H, et al. Bone morphogenetic protein 2 controls steroid-induced osteonecrosis of the femoral head via directly inhibiting interleukin-34 expression. *J Mol Endocrinol*. 2021;68(1):1–9. doi:10.1530/jme-21-0163
73. Sekar S, Crawford R, Xiao Y, Prasadam I. Dietary fats and osteoarthritis: insights, evidences, and new horizons. *J Cell Biochem*. 2017;118(3):453–463. doi:10.1002/jcb.25758
74. Peng P, Nie Z, Sun F, Peng H. Glucocorticoids induce femoral head necrosis in rats through the ROS/JNK/c-Jun pathway. *FEBS Open Bio*. 2021;11(1):312–321. doi:10.1002/2211-5463.13037
75. Fan ZQ, Bai SC, Xu Q, et al. Oxidative stress induced osteocyte apoptosis in steroid-induced femoral head necrosis. *Orthopaedic Surg*. 2021;13(7):2145–2152. doi:10.1111/os.13127